

Image Processing and Classification Applications in Aerospace NDT and Honey Bee Health Monitoring

Jiannan Zheng

A Thesis
In
The Department
of
Mechanical and Industrial Engineering

Presented in Partial Fulfillment of the Requirements
for the Degree of Master of Applied Science (Mechanical Engineering) at
Concordia University
Montreal, Quebec, Canada

December, 2012

© Jiannan Zheng, 2012

Concordia University

School of Graduate Studies

This is to certify that the thesis prepared,

By: Mr. Jiannan Zheng

Entitled: Image Processing and Classification Applications in Aerospace NDT and Honey Bee Health Monitoring

and submitted in partial fulfillment of the requirements for the degree of

Master of Applied Science

complies with the regulations of the University and meets the accepted standards with respect to originality and quality.

Signed by the final examining committee:

Dr. Javad Dargahi _____ Chair

Dr. Youmin Zhang _____ Examiner

Dr. Chun Wang _____ Examiner

Dr. Wenfang Xie and Dr. Lionel Birglen _____ Supervisor

Approved by _____

Chair of Department or Graduate Program Director

Dean of Faculty

Date _____

Abstract

Image Processing and Classification Applications in Aerospace NDT and Honey Bee Health Monitoring

Fast development in image processing and classification techniques brings many new solutions to the challenges in engineering. In this thesis, image processing and classification techniques are introduced as a powerful inspection tool into non-destructive testing on aircraft parts and honey bee disease detection to improve inspection speed and accuracy of human inspectors.

Safety and reliability are the most important issues in aerospace industry, especially in high temperature and pressure turbine engine parts. Fluorescent Penetrant Inspection (FPI) is widely used in Non-Destructive Testing (NDT) on aircraft parts as an easy and powerful method. To improve efficiency and robustness in human inspection in FPI, an Advanced Automatic Inspection System (AAIS) is developed by using image processing and classification techniques in this thesis. The system can automatically detect, measure and classify the discontinuities from turbine blade FPI images.

As the world's twelfth-largest honey producer, Canada's honey bee suffers from big losses in the past few years. The detection of disease and disorder of bee colony in an early stage is critical to prevent more loss for the bee industry. To greatly improve the speed of the inspection while retain accuracy, an automatic health monitoring system is developed to inspect honey bee colony and detect disease and disorder. The system can monitor colony development and measure the proportion of unhealthy cells. And thus it can improve the efficiency and accuracy of bee colony inspection significantly.

Acknowledgements

I would like to take this opportunity to express my deep gratitude to Concordia University. It's a great opportunity to study in this institution and to work on projects with these people. I am very grateful to my supervisors, Dr. Wenfang Xie and Dr. Lionel Birglen, and to all professors, students and partners in our group, for their support and guidance during my Master study.

I would also express my gratefulness to my dear parents and friends for their support and encouragement during my study here in Canada. Their unconditional love and bottomless support have made this thesis a reality. Also I would appreciate the financial and technical supports from industry partners: L3 communications, Pratt & Whitney and Novatek International.

Jiannan Zheng
Montreal Canada

TABLE OF CONTENTS

TABLE OF CONTENTS	V
LIST OF FIGURES	VII
LIST OF TABLES	XI
LIST OF SYMBOLS	XII
LIST OF ABBREVIATIONS	XIV
CHAPTER 1. INTRODUCTION	1
1.1 BACKGROUND.....	1
1.2 LITERATURE REVIEW.....	1
1.2.1 <i>Literature review on aerospace NDT</i>	2
1.2.2 <i>Literature review on honey bee colony health monitoring</i>	5
1.3 CONTRIBUTION OF THESIS	7
1.4 THESIS OUTLINE.....	8
CHAPTER 2. BACKGROUND KNOWLEDGE IN IMAGE PROCESSING AND CLASSIFICATION	10
2.1 INTRODUCTION	10
2.2 DIGITAL IMAGE ACQUISITION	10
2.3 COLOR MODELS.....	14
2.3.1 <i>RGB color model</i>	15
2.3.2 <i>Hue-Saturation-Intensity (HSI) color model</i>	15
2.4 BASICS OF INTENSITY TRANSFORMATION AND FILTERING.....	17
2.5 MORPHOLOGICAL OPERATION	19
2.6 NEURAL NETWORK CLASSIFICATION	21
2.7 CONCLUSION	23
CHAPTER 3. IMAGE PROCESSING AND CLASSIFICATION APPLICATIONS IN AEROSPACE NON-DESTRUCTIVE TESTING	25
3.1 INTRODUCTION	25
3.2 FPI TESTING.....	27
3.3 MAIN FUNCTIONS OF AAIS	30
3.3.1 <i>Image pre-processing</i>	31
3.3.2 <i>Image Segmentation</i>	34
3.3.3 <i>Feature Extraction</i>	38
3.4 CLASSIFICATION.....	44

3.5	SOFTWARE INTERFACE AND RESULTS	50
3.6	CONCLUSION	53
CHAPTER 4. IMAGE PROCESSING AND CLASSIFICATION APPLICATIONS IN HONEY BEE COLONY HEALTH MONITORING		54
4.1	INTRODUCTION	54
4.2	BROOD FRAME INSPECTION BOX.....	57
4.3	IMAGE PRE-PROCESSING	58
4.4	BROOD AREA DETECTION	60
4.4.1	<i>Edge filtering</i>	60
4.4.2	<i>Adaptive threshold with morphological transform</i>	62
4.5	BROOD AREA DETECTION	67
4.5.1	<i>Circular uncapped cells detection</i>	68
4.5.2	<i>Arc or fan-shaped uncapped cell detection</i>	69
4.6	ARTIFICIAL NEURAL NETWORK DECISION MAKING	70
4.7	SOFTWARE INTERFACE AND TEST RESULT	71
4.8	CONCLUSION	80
CHAPTER 5. CONCLUSION		81
5.1	SUMMARIZE OF RESEARCH WORK	81
5.2	FUTURE WORK	82
REFERENCES.....		84

LIST OF FIGURES

Figure 2.1 Human eye structure with Lens, Ciliary body and Retina [3].....	12
Figure 2.2 An example of human perceiving error – simultaneous contrast	12
Figure 2.3 An image of letter I shown as a 2-D matrix	13
Figure 2.4 Robot soccer players distinguished by different color signs (image from Carnegie Mellon University robot soccer team)	14
Figure 2.5 RGB color cube [3].....	15
Figure 2.6 HSI color model [3]	17
Figure 2.7 Image thresholding.....	18
Figure 2.8 Low-pass filter noise reduction.....	19
Figure 2.9 Examples of erosion and dilation functions with different SE.....	21
Figure 2.10 Structure comparison biological neuron and artificial neuron [6]	22
Figure 2.11 Structure of typical Multilayer perceptron [6]	23
Figure 3.1 System flowchart of AAIS	27
Figure 3.2 FPI chemicals: Water Washable Penetrant, Developer, Solvent Removable Penetrant and Solvent Cleaner (From left to right)	29
Figure 3.3 FPI inspection system: UV light, Camera and Computer (From left to right).....	29
Figure 3.4 Coupon after FPI process: under visual light (up) and under UV light (down)	30

Figure 3.5 Original RGB image, standard grayscale image and green component of original image (from left to right).....	31
Figure 3.6 Gamma function.....	33
Figure 3.7 Gamma Transformation results with $\gamma = 2$	33
Figure 3.8 Extract impulse signals from a 2-D signal using EDS: original signal (upper), background signal (middle), result signal (lower).....	35
Figure 3.9 EDS operation procedure and result	36
Figure 3.10 Result of image segmentation	38
Figure 3.11 4-neighbour connection check algorithm.....	40
Figure 3.12 Process of chain code.....	41
Figure 3.13 Minimum boundary box.....	42
Figure 3.14 Structure element of Thin function. X represents pixels not necessary to scan	43
Figure 3.15 Result of skeleton extraction with Thin function	44
Figure 3.16 ASTM-E433 Standard Reference Photographs for Liquid Penetrant Inspection.....	47
Figure 3.17 An indication is intersected with boundary of part	47
Figure 3.18 Hough transform maps points to m-c space	49
Figure 3.19 An example of Hough transform for line detection.....	49
Figure 3.20 Aligned indication detection: a complex case which the indication has several branches	50
Figure 3.21 AAIS software interface built in MATLAB GUIDE.....	51
Figure 3.22 FPI tests on coupon samples	52

Figure 4.1 A brood box with 10 man-made frames	55
Figure 4.2 A healthy brood sample.....	56
Figure 4.3 Inspection box with cameras.....	58
Figure 4.4 Convert a RGB brood frame image to standard gray scale image	59
Figure 4.5 Noise reduction by Median filter with Wavelet approach.....	59
Figure 4.6 Original image, gray scale image and histogram modification result.....	60
Figure 4.7 Canny edge detection result	61
Figure 4.8 Otsu adaptive thresholding result.....	63
Figure 4.9 Image erosion and reverse result.....	64
Figure 4.10 Result of brood boundary detection	65
Figure 4.11 Result of ellipse fitting function.....	66
Figure 4.12 Circular uncapped cells, noises and Arc or fan-shaped uncapped cells	68
Figure 4.13 Circular uncapped cells detection	69
Figure 4.14 Hough transform detect the arc or fan like uncapped cells	70
Figure 4.15 Software interface	72
Figure 4.16 Result of picture 1: Arc or fan-shaped uncapped cell detection.....	73
Figure 4.17 Result of picture 2: big noises from bees	74
Figure 4.18 Result of picture 3: low contrast and definition	75
Figure 4.19 Result of picture 4: Arc or fan-shaped uncapped cell detection.....	76
Figure 4.20 Result of picture 5: unhealthy brood with large number of uncapped cells.....	77

Figure 4.21 Result of picture 6: brood boundary interrupted by uncapped cells 78

LIST OF TABLES

Table 3.1 Comparison of average intensity of indication and background	32
Table 3.2 ASTM-E433 Standard Reference Photographs for Liquid Penetrant Inspection	45
Table 4.1 The TBC/TFC and BH/TBC percentage counted using software and manually	79

LIST OF SYMBOLS

R	Red component
G	Green component
B	Blue component
H	Hue value (HSI color model)
S	Saturation (HSI color model)
I	Intensity (HSI color model)
$T(.)$	Intensity transformation function
$f(x, y)$	Intensity of pixel (x, y)
k	Spatial filter
A	Input image
B	Structure element of morphological operation
γ	Gamma coefficient
$M(x, y)$	Result of Median filter of pixel (x, y)
g_{NH}	Edge points (Canny edge detection)
g_{NL}	Normal points (Canny edge detection)
g_{NM}	Potential edge points (Canny edge detection)

T_H	High threshold (Canny edge detection)
T_L	Low threshold (Canny edge detection)
R	Rectangularity
A_s	Aspect ratio
m	Slope
c	Intercept
ρ	Radial coordinate
θ	Angular coordinate
$\frac{TBC}{TFC} \%$	Percentage of brood cell in the whole frame area
$\frac{BH}{TBC} \%$	Percentage of unhealthy brood cell in the whole brood area
C	Circularity
(a, b)	Center of circle in spatial space (Hough circle transform)
r	Radius of circle in spatial space (Hough circle transform)

LIST OF ABBREVIATIONS

NDT	Non-destructive Testing
AAIS	Advanced Automatic Inspection System
FPI	Fluorescent Penetrant Inspection
MPI	Magnetic Particle Inspection
UT	Ultrasonic Testing
ECT	Eddy Current Testing
UV	Ultra-violet
RGB	Red-Green-Blue image format
BEMD	Bi-dimensional Empirical Mode Decomposition
FCM	Fuzzy C-Mean
CCD	Colony Collapse Disorder
ANN	Artificial Neural Network
HSI	Hue-Saturation-Intensity color model
SE	Structuring Element
VI	Visual Inspection
EDS	Erosion-Dilation-Subtraction operation

TBC	Total number of brood cells
TFC	Total number of frame cells
BH	Number of brood uncapped cells
BP	Back-Propagation training method

Chapter 1. Introduction

1.1 Background

The fast development in electronics industry as well as computer science has led to enormous progress in image processing and classification techniques in the recent years. Image and classification techniques can aid or even replace human labor in many applications. The tremendous increase in this area results in new solutions to many challenging problems in image analysis such as in manufacturing, civil engineering, biomedical engineering and geography. In this thesis, image processing and classification are introduced as a powerful inspection tool into aircraft parts non-destructive testing and honey bee health monitoring to help human inspector carry out the inspection and analysis work.

1.2 Literature review

In this section, a brief literature review on the image processing and classification, aerospace NDT and honey bee disease detection is presented and the motivation of the work undertaken in this thesis is given.

1.2.1 Literature review on aerospace NDT

In aerospace industry, safety and reliability are always the most important issues. Scientists and engineers pay lots of attention to damage analysis, product quality control and maintenance [7-14]. Among various parts, turbine engine parts especially turbine blades are the key parts to the in aircraft safety [16]. Regardless of the size of turbine blade, it is of crucial importance to keep the turbine blade free of defects since it transforms heat into power energy under extremely high pressure and temperature. Typical failure found on turbine blades can be classified into two categories: manufacturing failure and fatigue failure. Manufacturing failure is usually caused by the process of casting, solidification and coating while fatigue failure is caused by stress failure, thermal fatigue cracking and corrosion. All of them appear as surface discontinuities [17-20]. To investigate the failure, NDT methods can be applied to inspect the turbine blade.

As a powerful tool to detect and analyze structure failure and damage, NDT is widely used in aerospace, material and civil engineering. There are several NDT methods: Fluorescent Penetrant Inspection (FPI), Magnetic Particle Inspection (MPI), Ultrasonic Testing (UT) and Eddy Current Testing (ECT) [1-2]. MPI is to establish a magnetic field in a ferromagnetic material component and it can detect the defects on or near the surface. Imbert and Rampersad [23] successfully developed and tested MPI on small turbine blades, but MPI needs different coils for different shape and size of parts, and the performance can be affected by surface paint and the angle of magnetic field with the defect. UT is to send sound waves into a test piece to detect the possible discontinuities. It can detect deep defects with high accuracy and does not need any part preparation. However, UT only

works fine on large parts and structures such as turbine engine shaft [24] or even bigger one like wind turbine blade [25]. ECT is also a popular NDT method in aerospace industry. A coil will produce a magnetic field to generate alternate electrical current (Eddy Current) on the test piece. This current will produce another magnetic field and the inductance caused by this magnetic field can be measured to detect the defects. ECT is highly sensitive to surface or near surface defects, and it can inspect special structures automatically using the well-designed probe [26-29]. In [28], an automated ECT on turbine blades have been presented. Since the distance between the probe and the test surface should be kept the same during the whole ECT scan process, it needs special probe and well-tuned surface scan for every type and size of blades, and the speed of process is relatively slow [28]. For some parts like mounting holes [26], or turbine rotors [27], ECT process is easier to be automated, but for turbine blade testing, ECT is not the best option [30]. FPI is to apply liquid fluorescent penetrant to the surface of a test piece; the liquid is pulled into the defects by capillary action. Then the surface is cleaned and developer is applied to pull out the penetrant from the defects. The indication of defects can be seen under Ultra-Violet (UV) light source [30]. Compared to the other NDT methods, FPI is much cheaper and easier to apply, and better for inspecting the turbine blade with small surface defects and complex geometry. Besides, unlike the other NDT methods, FPI can process large surface area or large volumes of parts at the same time, which makes it the most efficient, lowest cost NDT method for turbine blades' defect detection with high sensitivity [31].

Automated FPI has already been developed by some major aerospace companies. Adair et al. from Pratt & Whitney have developed an Automated FPI process system with several processing stations in line to process the test pieces automatically [32]. Other

automated FPI systems are developed by some NDT companies with similar processing stations or tanks. Even though those automated FPI system can handle complex chemical process, the final visual inspection step is still done by human inspectors. An automated inspection system is needed to aid human inspectors' work of detection, measurement and classification.

In the literature many proposed image based defect inspection researches have been carried out on a variety of NDT applications that we can use for reference here. Image pre-processing, segmentation, feature extraction and classification techniques are discussed in those literatures [34-56]. To convert RGB image from imaging sensor to gray scale image, Nashat et al. decompose color information in RGB image and subtract to enhance crack indication [35]. In FPI inspection case, since FPI indication is in green, the green component is used to enhance the indication directly. For the further improvement of gray scale image quality, median filter noise reduction is introduced [34][36][39][51]. The most important and challenging part is the indication segmentation process which can be categorized into three groups: 1. Segment in intensity i.e. thresholding, 2. Segment in gradient i.e. edge detection and 3. Segment by subtraction approach. In [35][37][44][49] , the researchers use pre-tuned threshold and references [34][36] introduce adaptive threshold method – Otsu method [5], which has very good performance and robustness. In [36][37][40][47], the researchers applied Sobel filter for edge detection, while in the comparison made by [48], Canny filter is probably the best in edge detection for defect indications. In subtraction approach [49], the authors subtract a predefined background image of welding to segment crack indication. And in [36][46][50], low-pass filter is applied to smooth the original image to get background image. In [51], the background

image is obtained from an analytical software – TableCurve3D from IBM Statistical Package for the Social Sciences (SPSS). Other segmentation methods include local segmentation with edge detection [55] for welding image, which may not be very useful in turbine blade image inspection. And bi-dimensional Empirical Mode Decomposition (BEMD) [52] and Fuzzy C-Mean (FCM) [54] cannot achieve convincing results. In this thesis, we will investigate various image processing techniques, such as intensity thresholding, gradient edge detection and subtraction approaches for turbine blades' inspection. We have developed an Otsu Adaptive thresholding which combines Canny Edge Detection and Erosion-Dilation-Subtraction methods to achieve good quality indication image. The details will be discussed in Chapter 3. In feature extraction and classification step, we developed algorithms to measure and classify indications according to Liquid Penetrant Inspection Standard ASTM E433-71 [57][58].

1.2.2 Literature review on honey bee colony health monitoring

In Canada, honey bee industry is an important part of this country's agricultural production, makes Canada the world's twelfth-largest producer of honey [64]. According to recent research, Canadian bee keepers suffer from Colony Collapse Disorder (CCD) in the past few years [59]. Over the winter of 2008-2009, Canadian bee keepers lost 33.9% of colonies, twice the normal rate of winter losses. In some provinces such as Alberta, New Brunswick and Prince Edward Island (PEI), the number exceeds over 40% [60]. Many research and survey has been made on the CCD in the past few years, and two main causes

have been discussed: 1. bacterial disease – American foulbrood disease [63-64]; and 2. parasites disease – Varroa destructor [65][68] and Nosema [66]. However, there's no final conclusion in the debate of the major cause of CCD, and the only effective way to control CCD is to monitor bee colonies and to identify unhealthy bee colony in an early stage. Two approaches can be applied to monitor bee colony health condition: monitor individual bee for example the queen by video based image [67][68]; or inspect bee brood frame for healthy brood area and healthy cell percentage [69]. Compared with the first approach, the second one costs less in terms of equipment and gives more information in terms of healthy cell numbers and percentages. In addition, the visual inspection is very time-consuming, tedious, and inaccurate due to limitations of the human eye working under poor visibility conditions (full sun, shading by the beekeepers hat & veil, sweat dripping into eyes, eye glasses fogging up). For a beekeeper in Eastern Canada with 300 colonies, the inspection takes approximately 300 hours of work every 10 days. An automated solution is urgently needed for bee colony scanning and disease identification to improve the Canadian beekeeping industry. In this thesis, we built up an automated honey bee colony health monitoring system including both hardware and software systems. In hardware system, this thesis designed a brood frame inspection box to take brood pictures with uniformed high quality. In software system, this thesis developed an algorithm which combines Otsu adaptive thresholding [5] method with morphological operations [3] and ellipse fitting function [70] to extract brood boundary, and compared with edge detection method. Lee Hung Liew, Beng Yong Lee and Margaret Chan introduced circular Hough transform in cell detection [69]. However, circular Hough transform needs large amount of computation. In this thesis, we improved this algorithm's efficiency by introducing circularity detection

before applying Hough transform to avoid unnecessary computation. In the final decision making step, we used Artificial Neural Network (ANN) [6][34][56] to classify honey bee colonies' health condition into healthy or unhealthy conditions.

1.3 Contribution of thesis

In this thesis, image processing and classification techniques are applied to two different applications which share a common feature of detecting condition by using images.

In the design of an advanced automatic inspection system for turbin blade FPI analysis, the main contributions are listed as follows:

- A new approach is developed to perform automatic accurate segmentation of turbine blade indication from background after FPI process. This approach combines Otsu Adaptive Thresholding with Canny Edge Detection and Erosion-Dilation-Subtraction method.
- Special feature extraction and classification functions are designed to perform automatic classification of indications.
- A user friendly interface is designed to show detection and classification results of the advanced automatic inspection system.

In the design of an advanced automatic inspection system for honey bee colony health monitoring, the main contributions are listed as follows:

- A new simple and effective approach is developed to perform automatic brood boundary detection with high accuracy. This approach integrates Otsu Adaptive Thresholding and morphological operations.
- A new approach in uncapped cells detection is developed by integrating circularity detection and Hough circle detection.
- A user friendly interface is designed to show detection and classification results of the advanced automatic inspection system.

1.4 Thesis outline

The thesis is organized as follows.

In Chapter 1, background and motivation are introduced. The thesis outline is given as well.

In Chapter 2, a brief review on the background knowledge in image processing and classification is carried out. The basic fundamental principles in digital image acquisition and color models are presented. Spatial transform, filtering and morphological operation techniques are discussed. The classification technique ANN is described briefly at the end of this chapter.

In Chapter 3, image processing and classification techniques are applied to aerospace NDT applications. NDT and FPI methods are briefly reviewed and the challenge of automated FPI process is discussed. Then the image pre-processing techniques are

implemented to acquire good quality gray scale images. Image segmentation functions are developed to segment the indications from the background. Feature extraction functions and classification functions are implemented to measure and classify the indications. Finally, the sample images from industrial partners are tested by the developed system and the field work has been carried out.

In Chapter 4, image processing and classification techniques will be further carried on in a brand new field – honey bee health monitoring. First, some background of Canada's honey bee industry and situation of CCD are reviewed. In this thesis, a hardware inspection box is designed to take standard good quality pictures for honey bee brood inspection. A simple and effective brood boundary detection method is presented to accurately extract the brood area out of frame. Uncapped cell detection function using Hough transform and circularity detection is developed to detect the unhealthy cells inside brood area. Finally an ANN is trained and implemented in the system to make final decision on the brood health condition.

Finally, Chapter 5 concludes the thesis and gives the future work.

Chapter 2. Background knowledge in Image Processing and Classification

2.1 Introduction

In this chapter, we will review the background knowledge related to the research work which is carried out in this thesis. Image processing and classification techniques are implemented to inspect aircraft parts and honey bee brood to evaluate the health condition of those test pieces. This chapter starts with a brief introduction of basics of digital image acquisition, including human vision structure, digital image sensing, sampling and representation. Different colored image models will be discussed and compared thereafter. Spatial transformation, filtering and morphological operation techniques will be introduced as they are used to perform indication segmentation in this research. Finally, since both problems are treated as classification problem in this research, the classification tool – neural network will be reviewed at the end of this chapter.

2.2 Digital image acquisition

Visual ability is an important ability of human being. Information which collected from eyes consist a large proportion of all. With the evolution in computing and

information technology, digital image processing techniques have been developed and applied in a wide range of applications. Digital image acquisition is always the first step in digital image processing. As a matter of fact, digital image acquisition system is very similar to human vision system. When one talks about digital image acquisition, it always goes to human vision first.

In human vision, light goes through the lens and projects to the innermost of the eye, retina (Figure 2.1). The lens are supported and controlled by the fibers attached to the ciliary muscle. The focus of lens is changeable through ciliary muscle so that our eye can capture light from an object in a wide range of distance. Retina has millions of receptors: cones and rods. They are highly sensitive to color and can give us a full field of view. Human vision has certain advantages such as high color sensitivity and high brightness adaptation. However, shortcomings exist as well. The image perceived by our eyes is not simply dependent on the intensity and the shape of an object. A well-known example is simultaneous contrast, shown in Figure 2.2. The inner squares in those two pictures seem to have different brightness, but in fact, they have the same intensity. The same phenomena can be found in optical illusions, where people will see nonexistent or wrong information under some circumstances. Besides, the visible spectrum of human eye is narrow in the electromagnetic spectrum, which means that we could lose a lot of information as well.

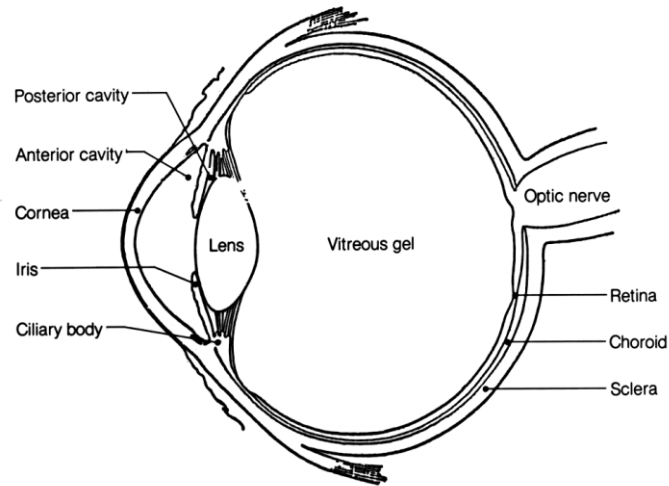


Figure 2.1 Human eye structure with Lens, Ciliary body and Retina [3]



Figure 2.2 An example of human perceiving error – simultaneous contrast

In digital image processing, the image is sensed and acquired by the sensors which have similar structure to human eyes. The light from the object goes through the lens and projects on an array of sensors. The lens is controlled by mechanical structures to change the focus. Each individual sensor can receive the energy from the light and transform this energy into a voltage signal. Since different electromagnetic spectrums result in different energy, the sensor will produce different signals to distinguish among different spectrums. Thus this enables the sensor to read all radio wave in electromagnetic spectrums including both visible and invisible lights. A sensor array consists of many sensors lying in a plane

which will give us a 2-D image. The resolution of a digital image is based on the numbers of sensors. Then, the voltage signal from sensor is converted from analog signal into digital signal by the means of sampling. Finally a 2-D image will be represented by a 2-D matrix.

(Figure 2.3)

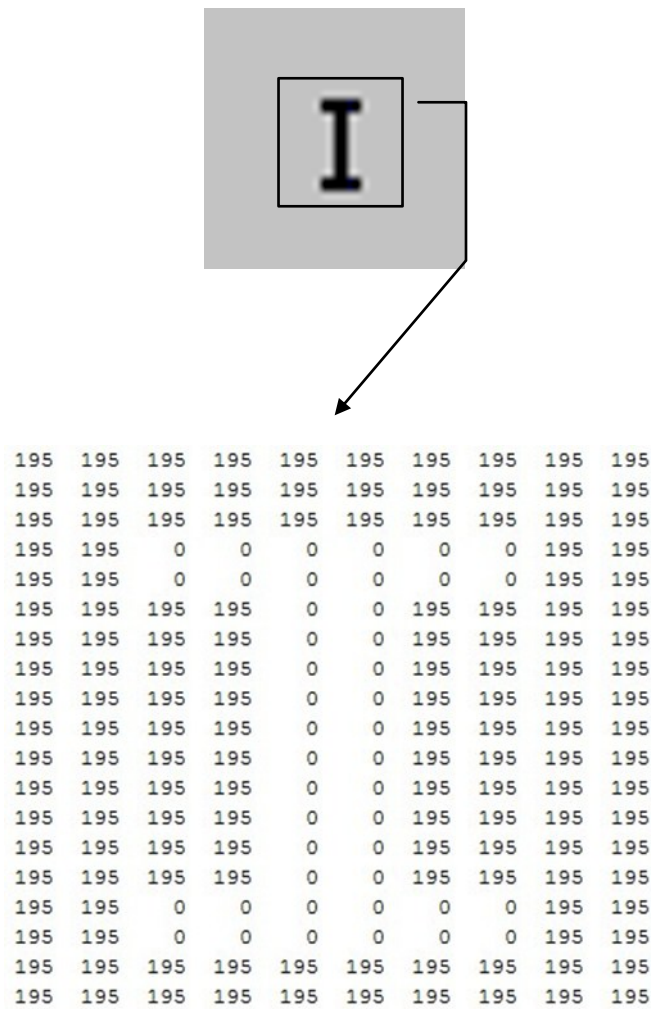


Figure 2.3 An image of letter I shown as a 2-D matrix

2.3 Color models

Color image processing is widely used in digital image processing and visual servoing tasks. The application is motivated by two main reasons: first, human vision system has the ability to recognize and distinguish thousands of colors as mentioned in the previous section. Second, the color is a powerful indicator which can simplify many image processing tasks. For example, in Figure 2.4, the robot soccer players are distinguished and located by different color signs on the top of them. The computer will analyze the images from top camera to know the position of each team member precisely. In this thesis, color information is a powerful indication in both applications. In this section we will review several color models in digital image processing.



Figure 2.4 Robot soccer players distinguished by different color signs (image from Carnegie Mellon University robot soccer team)

2.3.1 RGB color model

RGB color model is the most common model used in hardware devices such as digital cameras and digital monitors. According to research results, the cones in the human eye are sensitive to colors, and they can be classified into three main categories – the three primary colors: red (R), green (G) and blue (B). RGB image has three values in each pixel: R, G and B. In a standard 24-bit RGB image, every component has 8-bit range, 256 values, the combination will have $(256)^3 = 16,777,216$ different colors. Figure 2.5 shows the RGB color cube. In this thesis, color images will be taken and saved in RGB model for further analysis.

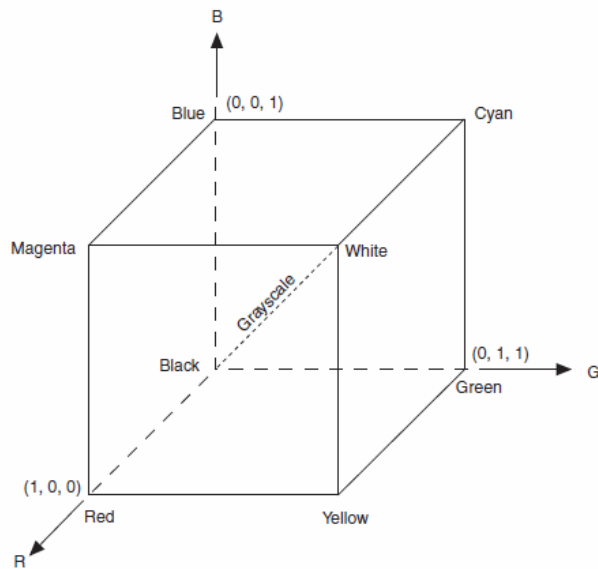


Figure 2.5 RGB color cube [3]

2.3.2 Hue-Saturation-Intensity (HSI) color model

RGB color model is perfect for image sensing and display, but when it is used to describe color, it's relatively weak. In a RGB image, we cannot tell the color directly from the R, G, B values. Compared with RGB color model, HSI can better present human interpretation of color. In HIS image, hue is the color property that describes the pure color, which will give us accurate color information of an object. Hue value is robust to light intensity and reflection angle changes. Saturation is the colorfulness of the pure color. And intensity is the measure of light which is reflected by the color.

Hue, saturation and intensity can be calculated from RGB value. As shown in Figure 2.6, HSI color model is cylinder like where the vertical axis is the intensity value, saturation value is the distance from the color point to the intensity axis, and hue is the angle the origin color—red. Equations 2.1 to 2.3 give the conversion from standard RGB model image to HSI model image [3].

$$H = \begin{cases} \theta, & B \leq G \\ 360 - \theta, & B > G \end{cases} \quad (2.1)$$

where $\theta = \arccos\left\{\frac{\frac{[(R-G)+(R-B)]}{2}}{[(R-G)^2+(R-B)(G-B)]^{\frac{1}{2}}}\right\}$.

$$S = 1 - \frac{3}{R+G+B} [\min(R, G, B)] \quad (2.2)$$

$$I = (R + G + B)/3 \quad (2.3)$$

where H is hue value, S is saturation and I is intensity of HSI color model.

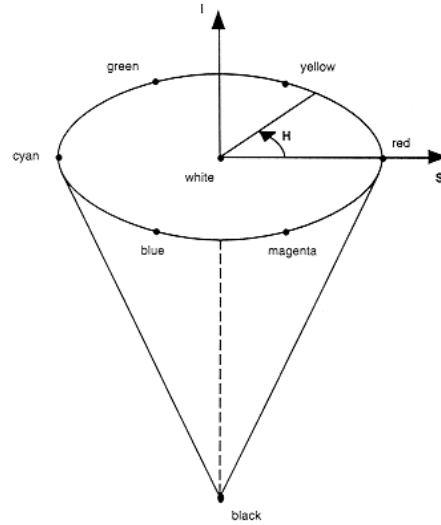


Figure 2.6 HSI color model [3]

Intensity value is the only descriptor of gray scale image or monochrome image. Gray scale image only carries intensity value, which makes it easier to interpret by the computers and simplifies the calculation at the same time. It is suitable for more complex image operations such as filtering and morphological operations. Equation 2.4 shows a typical RGB to gray scale image transformation function.

$$\text{Gray scale value} = 0.299 * R + 0.587 * G + 0.114 * B \quad (2.4)$$

2.4 Basics of intensity transformation and filtering

Intensity transformation and filtering are two main operations working in spatial domain, or in image plane. They change image pixels directly in their values. Intensity transformation can be used to improve the contrast of an image or to perform image thresholding. Spatial filtering can sharp or fuzzy an image, or perform edge detection as

well. In this section, we will introduce some basics of intensity transformation and filtering.

Intensity transformation is operating directly on every pixel of an image according to a certain rule. It can be described as in Equation 2.5,

$$g(x, y) = T(f(x, y)) \quad (2.5)$$

where $f(x, y)$ and $g(x, y)$ are the pixel values of input image and output image at position (x, y) , T stands for the transformation rule of the operation [3]. An example for intensity transformation is thresholding. In Equation 2.6, T is a typical thresholding function, if a pixel value is higher than 100, it has a new value 1, otherwise 0. This operation transforms a grayscale image into a bitmap image. (Figure 2.7)

$$T(i) = \begin{cases} 1, & i > 100 \\ 0, & i \leq 100 \end{cases} \quad (2.6)$$

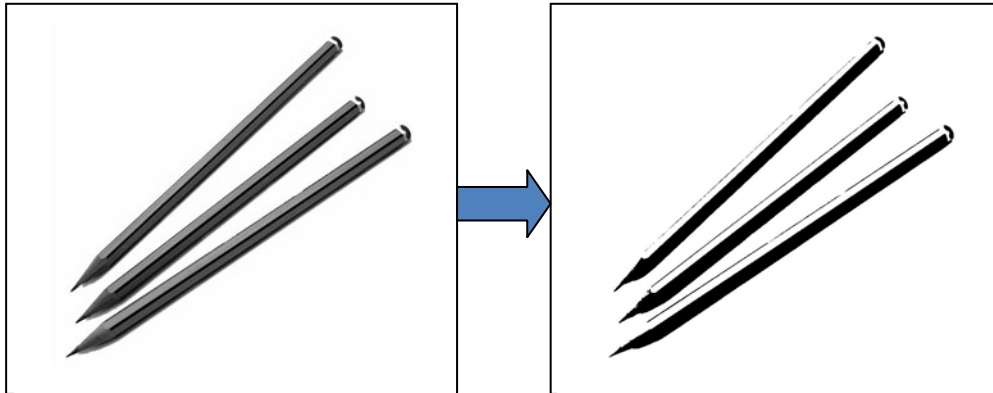


Figure 2.7 Image thresholding

Spatial filtering has the same function in Equation 2.5, but the function T will be a spatial filter k instead. In Equation 2.7, the spatial filter is a typical low-pass filter. Low-pass filter reduces high frequency signals such as noises and edge information of an image. This filter gives pixel (x, y) the average value of its 3x3 neighborhood pixels. The filter

will move from pixel to pixel and scan the whole image. Figure 2.8 shows an example of low-pass filter noise reduction.

$$k = \begin{bmatrix} 1/9 & 1/9 & 1/9 \\ 1/9 & 1/9 & 1/9 \\ 1/9 & 1/9 & 1/9 \end{bmatrix} \quad (2.7)$$

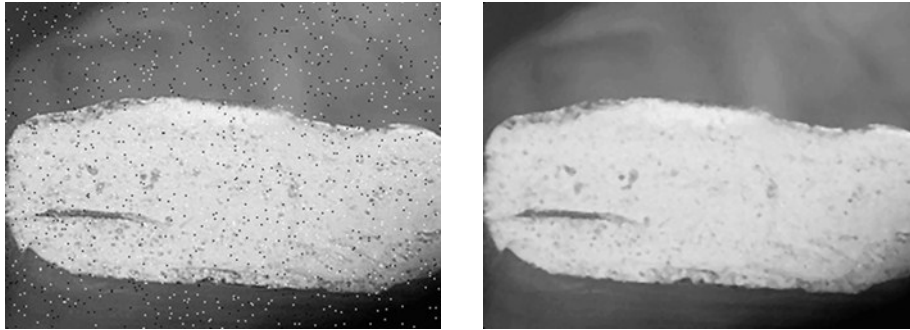


Figure 2.8 Low-pass filter noise reduction

2.5 Morphological operation

Morphological operation is a powerful approach in image processing other than spatial functions. It provides new solutions to numerous problems in image processing, such as extracting edge, thinning and filtering.

Morphological operation is based on set theory. In digital image processing, gray scale images are stored and represented as 3-D matrix. Every element has 3 components: x and y position and gray scale intensity. Morphological operation is performed by structuring elements (SE). SE is a small matrix or image. When one performs morphological operation, SE will be used to scan input image pixel by pixel and to create a new image. For example, erosion, a fundamental operation in morphological operation, is

used to shrink objects in an image. It is defined by Equation 2.8, where A is the input image, B is SE of erosion, i is the set of origin points of B contained in A [3]. Dilation operation is defined by Equation 2.9 [3].

$$A \ominus B = \{i \mid (B)_i \subseteq A\} \quad (2.8)$$

$$A \oplus B = \{i \mid (B)_i \cap A \neq \emptyset\} \quad (2.9)$$

Figure 2.9 shows the examples of erosion and dilation operation. The first image is eroded by a vertical line, and gives the result of two vertical lines of letter “H”. The second image is eroded by a square, and gives the result of a thinner “H”. The third image is dilated by a square, and gives the result of a bolder “H”. Through this example, we can see that a square SE can thin or thicken an object while a line SE can detect lines. In this thesis, morphological operations will be used in indication segmentation and feature extraction functions.

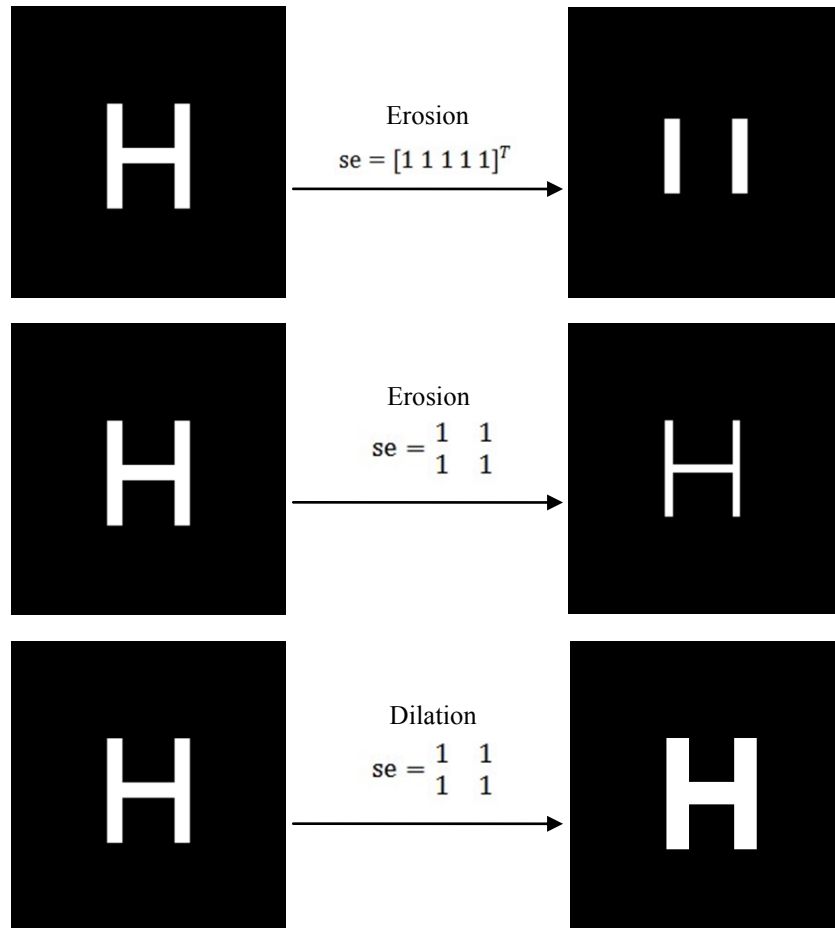


Figure 2.9 Examples of erosion and dilation functions with different SE

2.6 Neural network classification

Compared with normal digital computer, human brain computes in a much more complicated way. It is a highly complex and parallel computer made up with biological neurons. Artificial neural network is to simulate biological neural network's neuron, structure, reaction and learning algorithm to solve some nonlinear and complex tasks for which normal logical computing could not solve. In this section we will briefly review the

basics of artificial neurons and Multilayer Perceptron (MLP).

Biological neuron's functions are mainly accomplished by dendrites, cell body and axon. Dendrites are thin structures from the cell body and working as inputs to the cell body. Cell body analyzes signals from dendrites and gives output to axon. Axon connects to thousands of target cells through synapses. Artificial neuron has similar structure to that of biological neuron. As shown in Figure 2.10, it has a set of inputs and relevant weighting vector. An adder will sum all input signals and an activation function will make decision based on a threshold function. The output of artificial neuron will go to actuators.

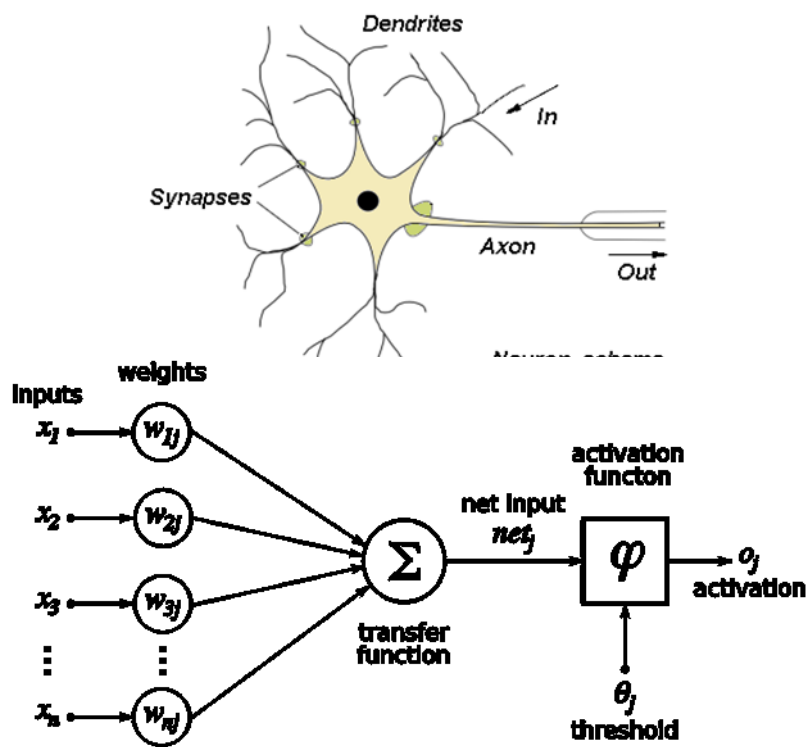


Figure 2.10 Structure comparison biological neuron and artificial neuron [6]

Multilayer perceptron is a typical feed forward artificial neural network which

consists of multiple layers: input layer, hidden layer and output layer. Each neuron in one layer connects with a certain weight to every neuron in the following layer. MLP exhibits a high degree of connectivity, means a neuron will be connected to all neurons from upper and lower layer (Figure 2.11). MLP is widely used in statistical estimation, classification, nonlinear control and image analysis. In Chapter 5, we will use MLP to classify healthy and unhealthy honey bee colony.

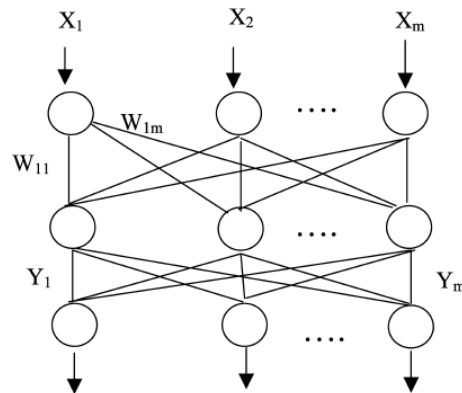


Figure 2.11 Structure of typical Multilayer perceptron [6]

2.7 Conclusion

In this chapter, the background knowledge and methods related to thesis work has been reviewed. First, with regards to image acquisition, human vision system, digital image sensing, sampling and representation have been reviewed. Different color models have been discussed to enhance the information of interest in images. Spatial transformation and filtering techniques have been presented as they are powerful tools in contrast enhancement and image segmentation. Morphological operations have been

reviewed through two examples: erosion and dilation. They are implemented in both problems for background segmentation and brood boundary extraction. Some basics of Artificial Neural Network are presented for the subsequent classification of the brood frame images in the honey bee colony health monitoring system.

Chapter 3. Image processing and classification applications in aerospace non-destructive testing

3.1 Introduction

In aerospace industry, safety and reliability are the most important concern. Very little defect or fault can cause catastrophic disasters. As a result, industry and research institutions pay a great deal of attention on product quality control and aircraft maintenance. Among a great number of parts, aircraft engine turbine blades are the most susceptible parts to defects as they work in extremely high pressure and temperature conditions. Regardless of its size, it is of critical importance in transforming heat into power energy. Its safety is always the first priority of aerospace industry.

In aerospace industry, preventive measures – NDT method is applied to detect discontinuities in an early manufacturing stage. NDT can evaluate a material, part or system without damaging the test piece. Common NDT methods are FPI, ECT, UT and MPI. Compared with the other popular NDT methods, FPI is comparably cheaper and more efficient for turbine blade detection than ECT and Ultrasonic. Thus it is suitable for detecting turbine blade surface discontinuities. However, FPI requires numerous labor forces in process, inspection and analysis procedures. Even though some automated FPI systems are already in operation to a certain extent with high quality, the final inspection

and evaluation of the FPI results are still carried out by human inspectors. Thus, advanced automatic inspection system is needed to ease the human inspectors' workload and to provide the inspection results precisely and efficiently.

In this chapter, we have designed and developed an Advanced Automatic Inspection System (AAIS) particular for FPI analysis to aid human inspector. The sample images of FPI turbine blade and coupons are taken under ultraviolet light after automated FPI process. Typical indications are bright green in various types, such as cracking, dusting, pit, cold shut, hot tear and so on. To accomplish the task of detecting and classifying indications from complex background and noise in turbine blade FPI images, we have developed an AAIS which contains 4 function parts: image processing, image segmentation, feature extraction and classification. In image processing, we compare the standard RGB to grayscale function with color components method, combine wavelet with median filter noise reduction, and enhance processing results with Gamma transformation. In image segmentation, we combine intensity thresholding, gradient edge detection and subtraction approach together. We develop an Otsu Adaptive Thresholding with Canny Edge Detection and Erosion-Dilation-Subtraction method to achieve the indication image with good quality. In the end, we develop feature extraction and classification functions to realize a preliminary classification function to classify indications into 2 types and 4 classes according to ASTM E433-71 liquid penetrant inspection standard. Figure 3.1 shows the flowchart of AAIS.

In this chapter, we will first review the basics and procedures of FPI testing in Section 2. The main functions of AAIS: image preprocessing, image segmentation, feature extraction and classification will be discussed in Section 3. In Section 4, the results from

sample turbine blade images and field testing will be given and analyzed. A software interface will be introduced as well.

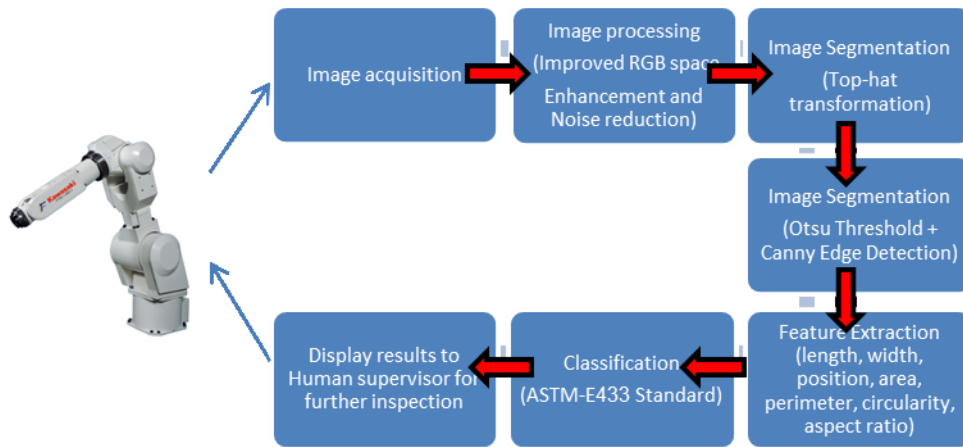


Figure 3.1 System flowchart of AAIS

3.2 FPI testing

FPI is one of the most widely used NDT methods in aircraft maintenance. FPI is a chemical procedure designed to detect surface discontinuities on nonporous specimen. In some critical parts like engine parts, small discontinuities are important to their safety. Discontinuities' length commonly ranges from 0.1mm to 5mm. The discontinuities in this kind of size cannot be discovered by human Visual Inspection (VI). The contrast between the discontinuities and the background surface is normally too small to be distinguished by human eyes. FPI can solve this problem by applying fluorescent liquid on the surface of specimen to increase the contrast between discontinuities and background so that they can be observed under UV light by human inspectors.

When applying FPI, surface preparation is usually the first step. One must make

sure that the surface is free of any contaminants that may restrict liquid penetrant to enter the discontinuities. Water, oil or other chemicals remain on the surface may mask the discontinuities. In order to clean the specimen, solvent cleaner and ultrasonic cleaner are applied. After cleaning, liquid penetrant will be sprayed on the surface. Because of surface tension, liquid will seep into small discontinuities slowly. After certain dwell time (around 30 minutes), penetrant remain on the surface should be removed by solvent cleaner. This step is critical and tricky since one should remove all surface penetrant but not inside the discontinuities. Lack of cleaning will bring lots of noises, and over cleaning will remove penetrant inside the discontinuities. The developer will be applied to make the penetrant inside discontinuities start to bleed out. This will make discontinuities visible by human eyes under UV light.

In this research, we use “SPOTCHECK” penetrant inspection products from Magnaflux (Figure 3.2). Specimen will be viewed under UV light; and a camera is connected to the computer to acquire FPI results (Figure 3.3). In Figure 3.4, a coupon is processed and viewed under UV light.



Figure 3.2 FPI chemicals: Water Washable Penetrant, Developer, Solvent Removable Penetrant and Solvent Cleaner (From left to right)

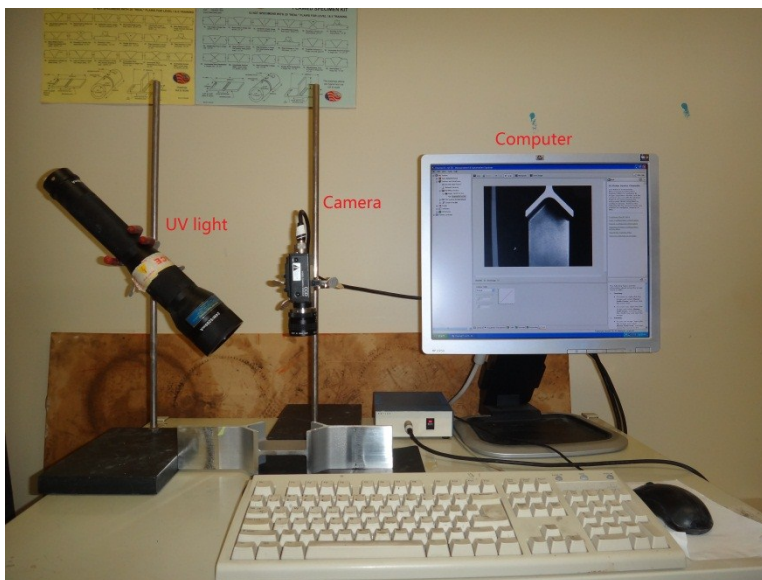


Figure 3.3 FPI inspection system: UV light, Camera and Computer (From left to right)

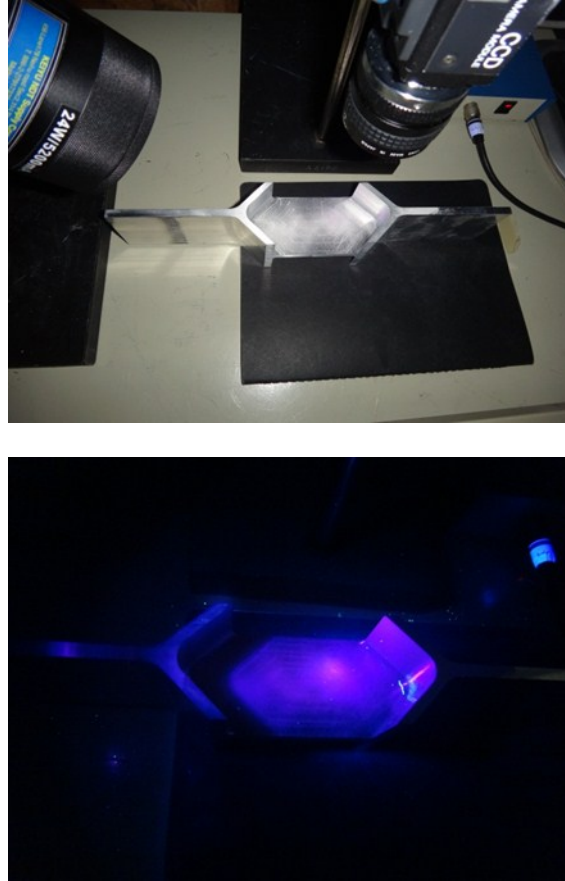


Figure 3.4 Coupon after FPI process: under visual light (up) and under UV light (down)

3.3 Main functions of AAIS

The main functions of AAIS include four parts: image pre-processing, image segmentation, feature extraction and classification. In this section, we will present those four functional parts in detail.

3.3.1 Image pre-processing

FPI result images are standard RGB images with similar color scales. The indications are bright green, and background is comparatively dark. Instead of using standard RGB to grayscale function (Equation 3.1), we found that green components from the original RGB image can enhance the green indications in FPI result image. The grayscale images results are shown in Figure 3.5. The comparison of average intensity from those results is shown in Table 3.1. As we can see, for the bright green indications in this research, green components are better than standard grayscale function.

$$\text{Gray scale value} = 0.299 * R + 0.587 * G + 0.114 * B \quad (3.1)$$

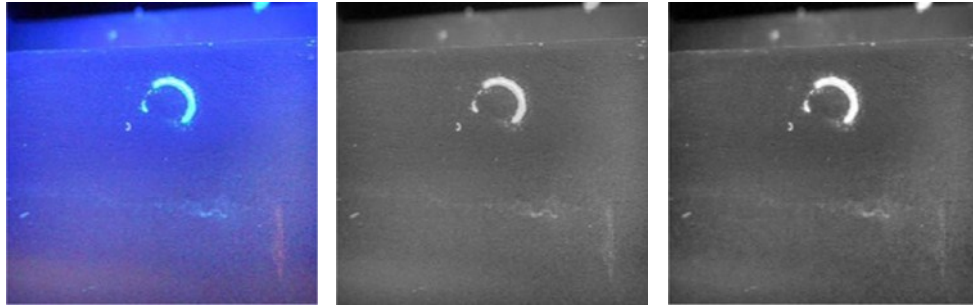


Figure 3.5 Original RGB image, standard grayscale image and green component of original image (from left to right)

Table 3.1 Comparison of average intensity of indication and background

	Standard grayscale image	Green component
Average intensity of indication	170.4089	190.8453
Average intensity of background	96.3360	85.5783
D-value	74.0729	105.2670

To further enhance the grayscale image, we use intensity transformation function mentioned in Chapter 2. The intensity transformation works on single pixels and can map input intensities according to a given function. The “Log” Transformation and “Gamma” Transformation (Equations 3.2 & 3.3) can easily enhance the intensity range of interest and reduce the influence from background information (Figure 3.6). In this case, we want to have less details from background image (lower intensity values) while retain the indications (higher intensity values). Figure 3.7 shows the Gamma Transformation results with $\gamma = 2$.

$$T(f(x, y)) = c * \log[1 + f(x, y)] \quad (3.2)$$

$$T(f(x, y)) = c * f^\gamma(x, y) \quad (3.3)$$

where c is a constant, $f(x, y)$ is the intensity value of pixel (x, y) .

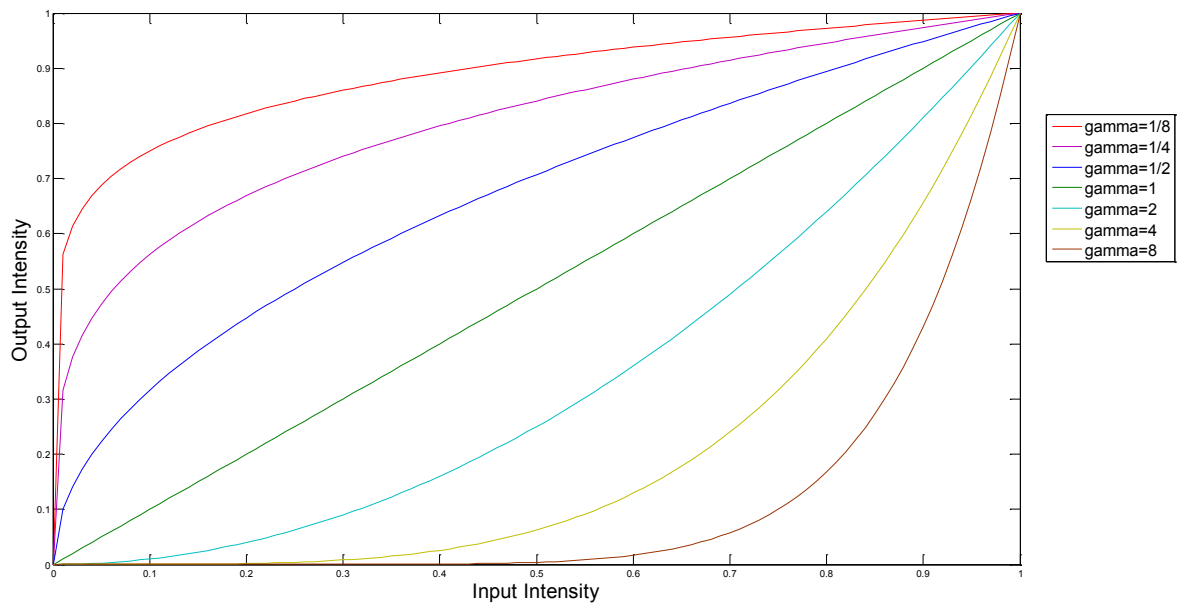


Figure 3.6 Gamma function

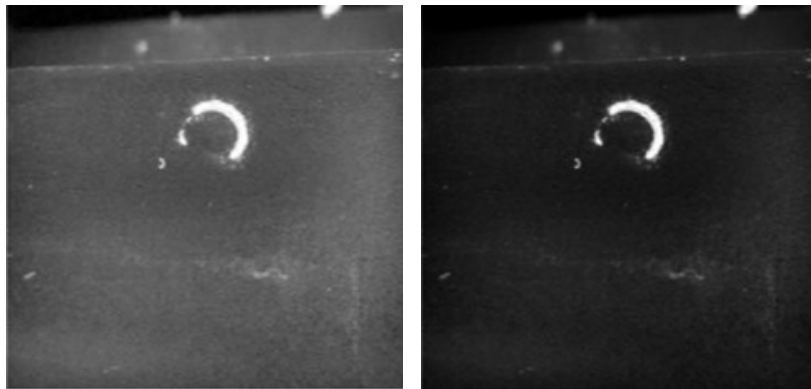


Figure 3.7 Gamma Transformation results with $\gamma = 2$

In the real situation, we may have some noises in the image. There are different kinds of noise reduction methods, and low-pass filter is the simplest one. However, it may bedim some edge information as well. Median filter is a very effective method in noise reduction, and it can reduce noise well and keep the edge information. In the project, we implement median filter noise reduction function. A 3-by-3 Median filter can be defined in

Equation 3.4,

$$M(x, y) = \text{median}\{z_k | k = 1, 2, \dots, 9\} \quad (3.4)$$

where z_k represents pixel (x, y) and its 8-connected neighbor pixels.

3.3.2 Image Segmentation

After being applied the image pre-processing steps in the previous section, the grayscale images now have good contrast without noise. Image segmentation functions can be carried out to extract region information thereafter. Image segmentation is the technique to divide target image into constituent regions. In this project, image segmentation functions will extract the indications from the background. An Otsu Adaptive Thresholding with Canny Edge Detection and Erosion-Dilation-Subtraction operations are developed and will be discussed in this section.

Erosion-Dilation-Subtraction (EDS) method is to extract the background image from original image first, and then to subtract with original image to get the foreground image. For example, if we are only interested in impulse signals like points A and B in a 2- D signal as shown in Figure 3.8, EDS will first obtain background signal, then do the subtraction to generate the signal of interest. The result in Figure 3.8 only keeps the impulse signals that we are interested in A and B .

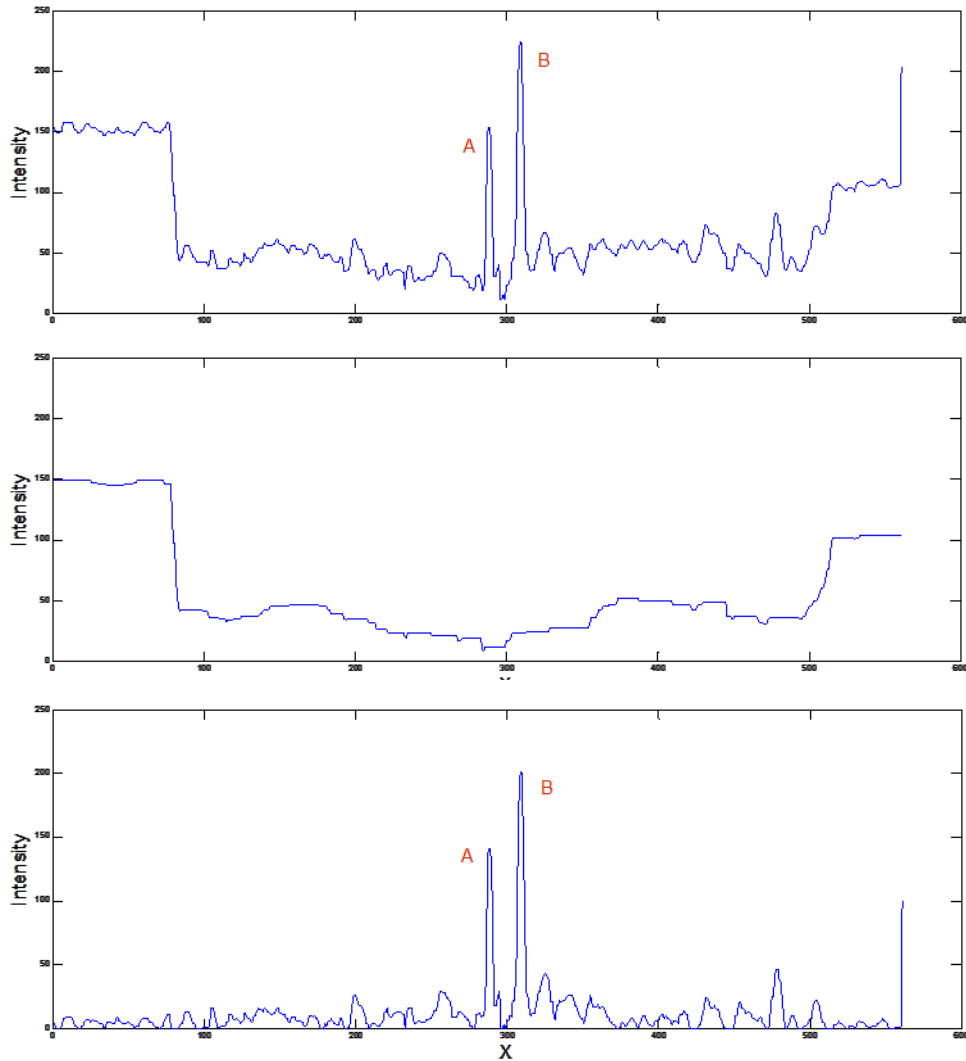


Figure 3.8 Extract impulse signals from a 2-D signal using EDS: original signal (upper), background signal (middle), result signal (lower).

Normally, in 3-D image processing, the background image will be obtained from curve fitting or surface fitting software. In this chapter, we have applied an advanced morphological operation method which combines erode operation and dilate operation (Equations 2.8 & 2.9) together to eliminate foreground indications and extract background image. As mentioned in Chapter 2, Erosion operation can thin an object in image while

dilation operation can thicken the object. With appropriate size and shape of operation structure element SE, we can eliminate the indications first in erosion operation, and then rebuild the background image with dilation operation. By this mean, we can segment background image and foreground image while introducing less additional information. Figure 3.9 shows the EDS operation procedures and results.

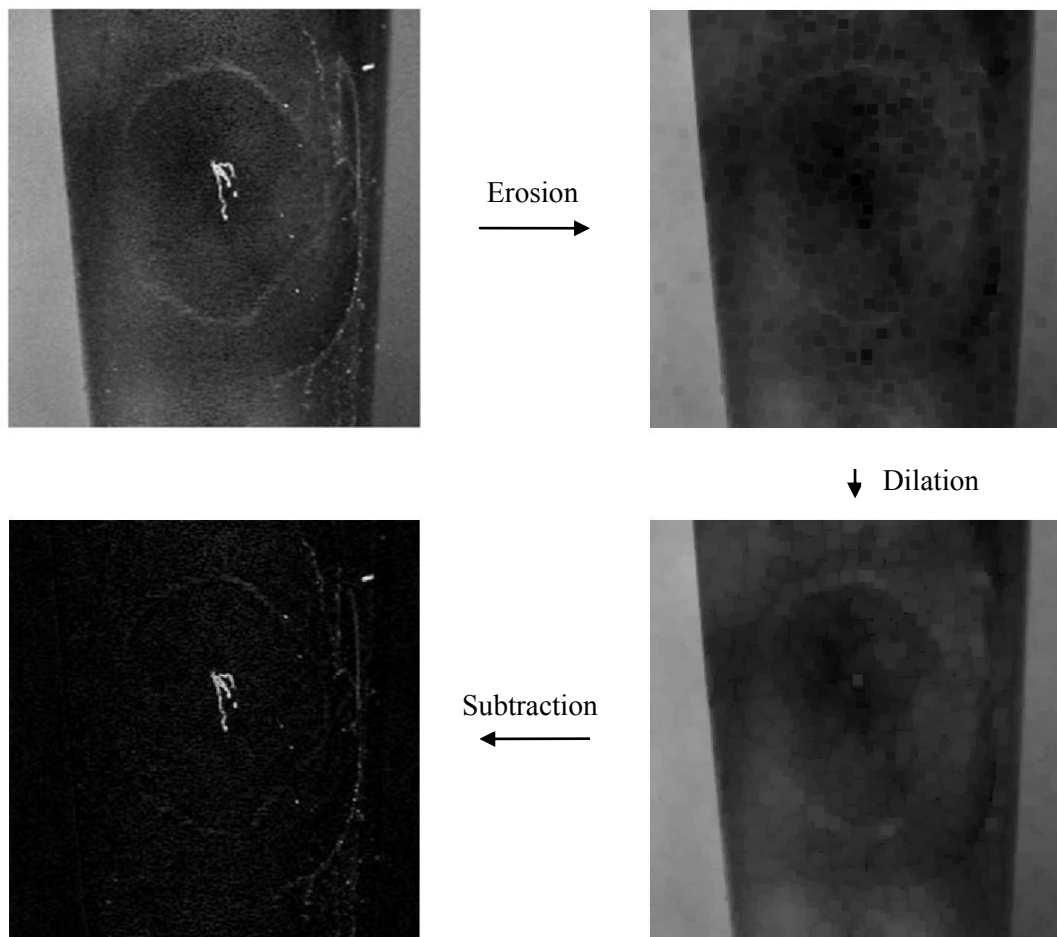


Figure 3.9 EDS operation procedure and result

After applying EDS operation, we can obtain foreground image in gray scale. In

this gray scale image we have the desired indications and plenty of noises (i.e. penetration remains on the surface) that will mislead the system to make wrong decisions. To improve the accuracy, it is necessary to do a further thresholding segmentation step to discard the noises and keep the indications as much as possible. To do this we combine Otsu adaptive threshold method together with Canny edge detection method, to set up two thresholds both in gray value intensity and gradient.

Thresholding is very useful in image processing to segment gray scale image into binary image. In this section, thresholding is used to obtain binary information of indications from gray scale foreground image. In intensity space, Otsu adaptive threshold method is based on the histogram analysis of the gray scale image. This method first assumes a threshold to classify pixels into two intensity groups, and then computes the between-class variance to maximize this value. The maximum between-class variance ensures that the threshold can separate pixels into two classes in intensity accurately, i.e. the foreground indications and background.

Edge detection is another effective approach in image segmentation. This approach segments the image in gradient space. Typical edge detection methods are Robert, Sobel and Canny edge detection. Compared with the other two methods, Canny edge detection performs better edge detection by its double thresholding and connectivity analysis. Canny method first applies a Gaussian filter to smooth the image, where the user can choose according to the size of objects. Then it computes the image into gradient map. After selecting two thresholds T_L and T_H , the algorithm considers the pixels with gradient higher than T_H to be edge points g_{NH} , while the pixels with gradient lower than T_L are treated as normal points g_{NL} . Finally, Canny method checks the 8-neighbor connectivity in the pixel

group g_{NM} with gradient higher than T_L and lower than T_H to connect the isolated edges.

Figure 3.10 shows the final result from image segmentation.

$$g_{NH}(x, y) = g_N(x, y) \geq T_H \quad (3.5)$$

$$g_{NL}(x, y) = g_N(x, y) \geq T_L \quad (3.6)$$

$$g_{NM}(x, y) = g_{NL}(x, y) - g_{NH}(x, y) \quad (3.7)$$

where g_N is the gradient value of pixels, g_{NH} , g_{NL} and g_{NM} are the three pixel groups classified by T_H and T_L .

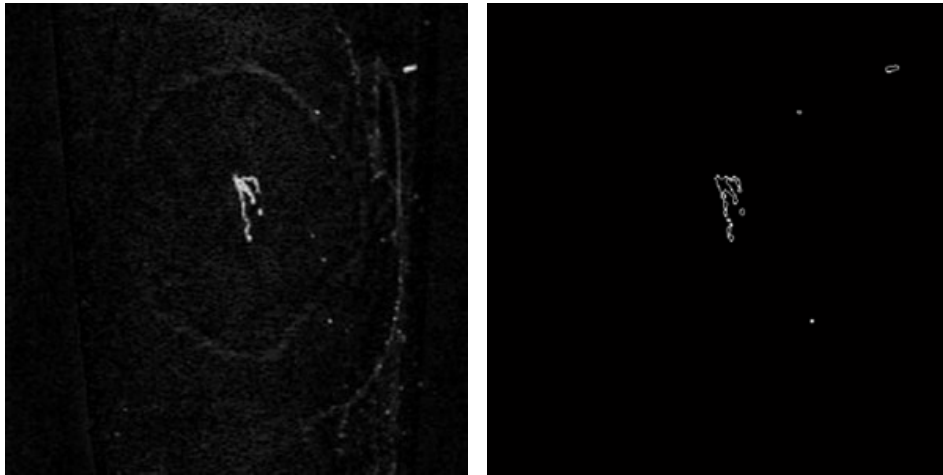


Figure 3.10 Result of image segmentation

3.3.3 Feature Extraction

In the previous sections, we have discussed about image processing and image segmentation functions. By applying those functions, AAIS can process the original image

to obtain the image with the indications in bitmap image. In this section, feature extraction functions are introduced to measure the indications. The results of feature extraction will be used in classification functions and for aiding human inspector for further detection.

The first thing of feature extraction is the boundary following process using 8-neighbour detection or chain code. Then the system can measure the object which is encircled by the detected boundary. Most of the detected objects represent the potential defects. The useful features are center position, length and width, area, minimum enclosing rectangle, aspect ratio, perimeter, rectangularity. In this section we will discuss border tracing, minimum bounding box detection, length, width and aspect ratio.

a Border tracing

Border tracing is to detect and label each object in one image. The result can be used for further feature extraction process. In Section 3.4, we have already obtained the image processing result in bitmap image. The value of indication pixels is 1 (white) and the background is 0 (black). To perform border tracing function we first remove all interior pixels and leave only boundary pixels. 4-neighbour connection check can detect interior pixels and remove them. Figure 3.10 shows how 4-neighbour connection check works. If all 4-connected neighbour pixels of the center pixel are 1, the center pixel is considered to be an interior pixel, and the algorithm will remove it.

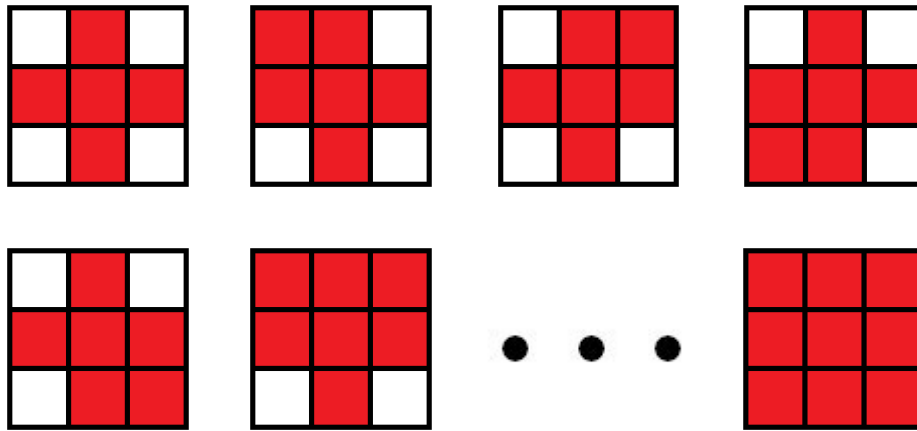


Figure 3.11 4-neighbour connection check algorithm

Border tracing can be performed by 8-neighbour connection check which is carried out in the following steps:

1. Scan for the top-left pixel as start pixel of each object O_i . For object O_i , mark the start pixel by giving a new pixel value $i + 1$.
2. Start from left neighbor of the detected boundary pixel and perform 8-neighbour connection check in clockwise direction. If a new boundary pixel is detected and has value 1, record its position and assign value $i + 1$ to it.
3. Repeat step 2 until no more new boundary pixel is detected.
4. Repeat step 1, 2 and 3 until all pixels in the target image have been scanned.

In the resulted image, all boundary pixels will be detected. Boundary pixels from object O_i will have its only pixel value $i + 1$ as a label to distinguish between each object.

When one records and restores the location of boundary pixels, the chain code is very useful and efficient since it represents each position in only 8 digits. Figure 3.11

shows the operation of chain code. The code of this step is 7.

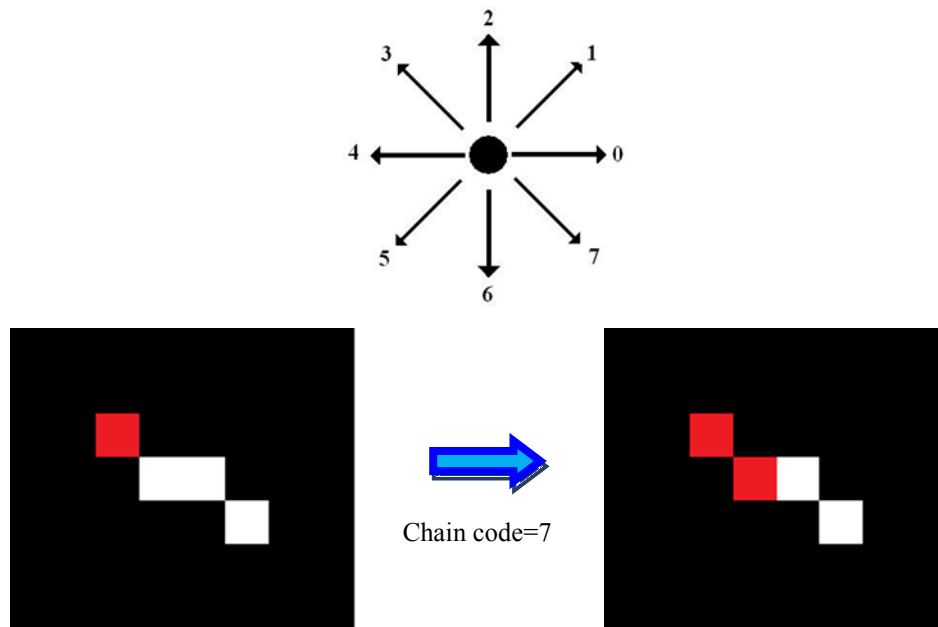


Figure 3.12 Process of chain code

b Minimum bounding box

After applying the boundary following process, the system detects all objects in image. Then it's possible to measure the indication represented by the objects. The minimum bounding box can measure the round and rectangular indications in length, width, center position and rectangularity. In this section, we will explain the minimum enclosing rectangle detection.

The minimum bounding box is the smallest rectangle that encloses the objects in the bitmap image. It can measure the objects' center position, length and width, orientation and rectangularity. As we have obtained boundary points in the previous section, we can

first select one point as starting point, scan the other boundary points and calculate the distance between them. Then the algorithm goes to the next starting point. After all points are scanned as starting point, we may find the longest distance between two boundary points. These two points are the endpoints of the main axis of this object and the distance is the length (Figure 3.12). We can scan the remaining boundary points and calculate the distance between the points to the main axis, select the longest distance from both sides of the main axis as the width of the minimum boundary box.

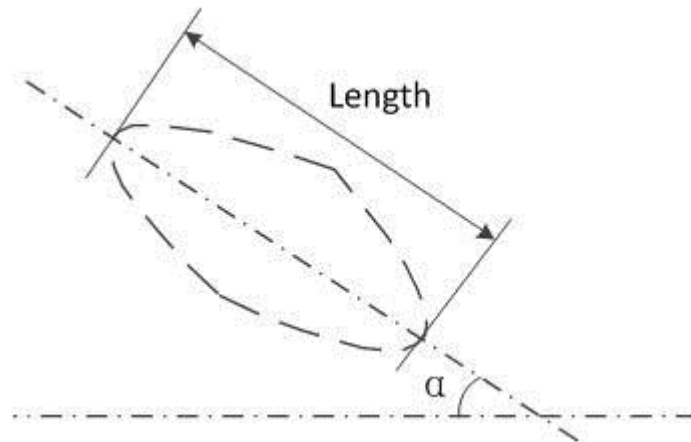


Figure 3.13 Minimum boundary box

Rectangularity is a measurement reflects the shape of the object. It's the relationship between the area of object and the area of the minimum bounding box (Equation 3.8). It ranges from 0 to 1. It takes on a maximum value of 1 for rectangular defects, $\pi/4$ for circular objects and becomes small for slender or curved objects like cracks.

$$R = \frac{A_o}{A_R} \quad (3.8)$$

where A_O is the area of the object, A_R is the area of the minimum bounding box.

c Length, width and aspect ratio

For round or rectangular indications, the length is the longest straight-line distance of the indication. It can be measured by the minimum bounding box of the object as mentioned in the previous section. But in some cases in this chapter, we may have the indications such as crack whose length is not the same as the minimum enclosing rectangle's length, but represents the path of the crack. Hence we need to find the length of this type of object. One effective way is to generate skeleton out of the object by using **Thin** function.

Thin function is a morphological operation which can thin an object to its skeleton. **Thin** function is to erode the target object by rotating structure elements shown in Figure 3.11. The algorithm continues performing the erosion function until no further change occurs in the target object. Figure 3.12 shows the result of **Thin** function.

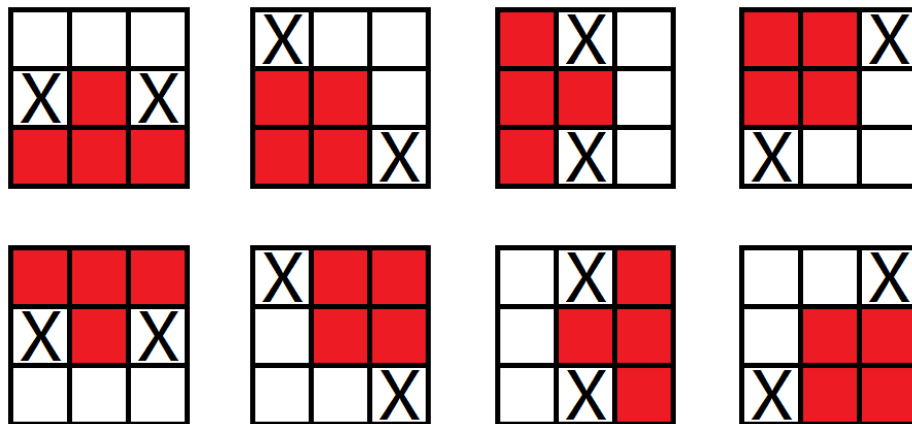


Figure 3.14 Structure element of **Thin** function. X represents pixels not necessary to scan

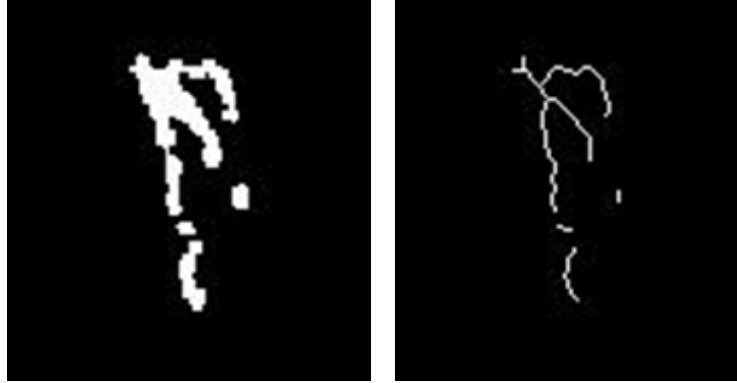


Figure 3.15 Result of skeleton extraction with **Thin** function

From the skeleton image, the system can measure the length of the indication accurately. With the length and area of the indication, we can calculate the approximate width of the indication by Equation 3.9. The aspect ratio is defined by Equation 3.10, which is a critical value measuring the sharpness of the indication.

$$W_A = A/L \quad (3.9)$$

$$A_s = L/W_A \quad (3.10)$$

where A and L are the area and length of an indication respectively.

3.4 Classification

With the features extracted from bitmap images, the system now can perform classification functions. In this specific problem, we have plenty types of indications from turbine blade, such as typical cracking, dusting, pit, cold shut, hot tear and dross. With the

features extracted from FPI process, it is impossible to classify all the indications into specific classes. In this thesis, we perform preliminary classification to classify the indications into 2 types and 4 classes, according to ASTM-E433 Standard Reference Photographs for Liquid Penetrant Inspection reapproved in 2003 [57].

ASTM-E433 Standard Reference Photographs for Liquid Penetrant Inspection is a specific standard set for classifying and characterizing indications detectable by penetrant inspection method, which is adopted in this thesis. The detailed classification criterion is showed in Table 3.2.

Table 3.2 ASTM-E433 Standard Reference Photographs for Liquid Penetrant Inspection

Type		Class	
I	Neither dimension is greater than three times the other.	A	Single
		B	Multiple unaligned
II	One of the dimensions is greater than three times the other.	C	Multiple aligned
		D	Intersection of surfaces

ASTM-E433 standard will classify indications into two types, Type 1 round/rectangular indications and Type 2 slender indications. We can refer to aspect ratio S mentioned in the previous section. If $S < 3$, the indication is Type 1, otherwise the indication is Type 2.

The Single and Multiple indications classification is to detect whether there are several indications in the same user defined area. In this thesis, instead of scanning every

part in the image, we only scan the areas in the neighborhood of each indication. The algorithm traverses all the indication detected in previous sections, applies N times of dilation operation to each of them to create the nearby areas, and verifies if those areas are connected to each other. If so, those indications are classified as multiple indications. The number of dilate operation times N can be chosen by human supervisor.

Figure 3.14 shows an example of multiple indication detection. First the algorithm selects one indication in the top left picture as initial object, and then performs dilation operation to create a nearby area for initial object as shown in bottom right picture. Finally, the resulted neighborhood area will be applied to the input image. If there are any other indications in the area, they will be classified as multiple indications or group indications.

Class D: indication intersects with boundary, the algorithm needs to be able to define the boundary of the part. We can refer to the results from previous Section 3.3.2: Image Segmentation. In that section, we successfully segment the foreground and background image from the input image. In the background image we can easily find the boundary of the part by applying edge detection. By matching two images together we can detect the intersections between indications and boundaries (see Figure 3.15).

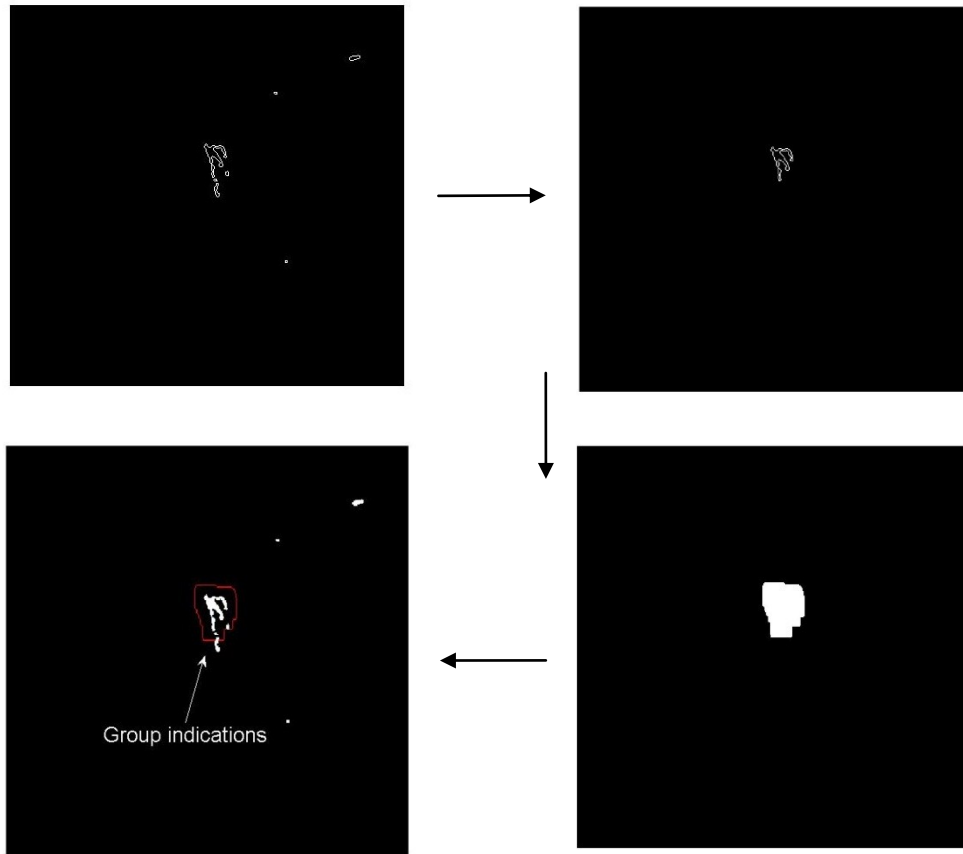


Figure 3.16 ASTM-E433 Standard Reference Photographs for Liquid Penetrant Inspection

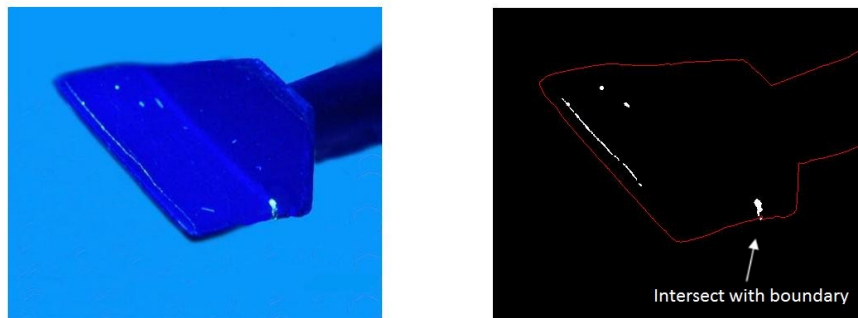


Figure 3.17 An indication is intersected with boundary of part

The most difficult classification is to classify between Class B and Class C, i.e. to classify the multiple indications into unaligned and aligned class. Here we implement Hough transform for line detection.

When we look at an image, it is a 2-D or 3-D matrix in spatial space. Every point in the image has x — y position and its intensity value. It is easy for human eye to recognize the color and shape, while relatively hard for machine. In order to overcome this problem, Hough transform can map image in spatial space into parameter space to perform particular shape detection. For example, in this project, the algorithm is expected to detect the close parallel lines in an image. Hough transform's solution is to transform this image into m - c space where m is the slope and c is the intercept (Figure 3.16). In the x - y space, the points share the same m and c values if they are on the same line. In m - c space, point (m_i, c_i) stand for a line in x - y space. If the value at point (m_i, c_i) in m - c space is n , that means we have n points on line (m_i, c_i) in x - y space. In x - y space, we can detect the line (m_i, c_i) (Equation 3.11). In the real situation, the difficulty lies in that m can be infinity, i.e. line $x=2$ can't be present in m - c space. So usually Equation 3.12 is used to transform x - y space into a polar coordinate space: ρ - θ space. ρ is the radial coordinate and θ is the angular coordinate. In this case ρ and θ can represent every possible line in x - y space. Figure 3.17 shows an example of Hough transform in detecting the long side and short side of rectangles. In the parameter space, 16 highlight points at $\theta = 0^\circ$ stands for 16 long side lines in the original image.

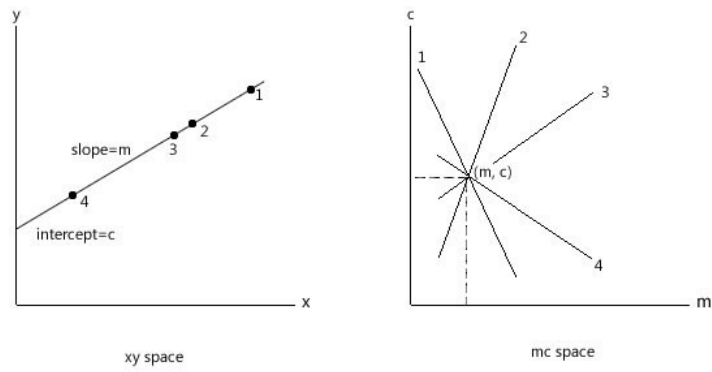


Figure 3.18 Hough transform maps points to m-c space

$$y = m * x + c \quad c = -m * x + y \quad (3.11)$$

$$\rho = x * \cos\theta + y * \sin\theta \quad (3.12)$$

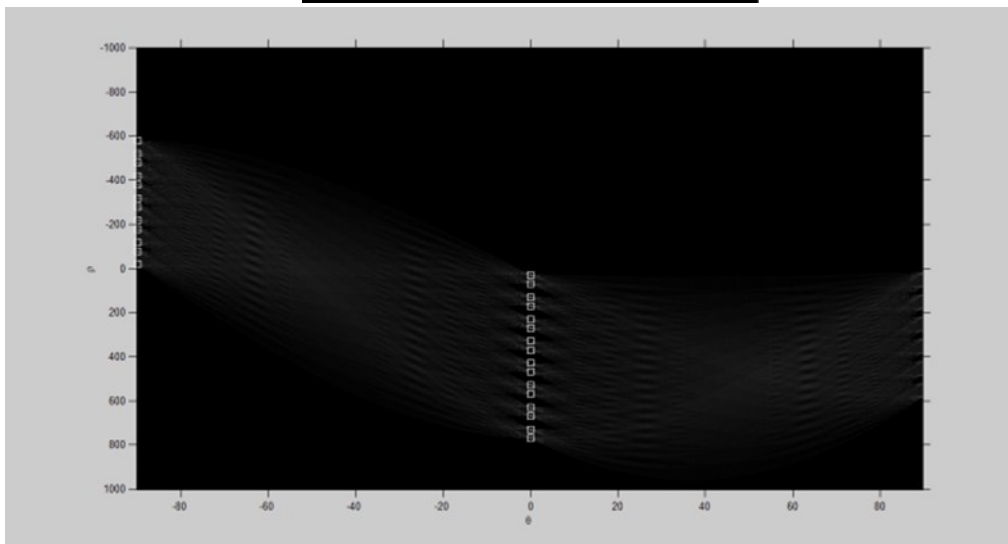
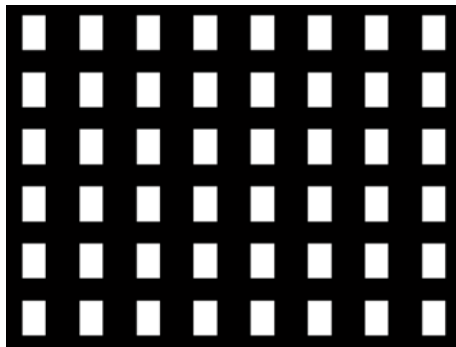


Figure 3.19 An example of Hough transform for line detection

In this thesis, we detect the aligned indications by performing Hough line detection from skeletons extracted in Section 3.3.3 Feature Extraction. By measuring the distance of points in parameter space, we can measure the closeness of two linear skeletons. For some complicate indications which have branches, we divide the indication into branches then perform Hough line detection. Figure 3.18 shows the detection of a branch with the other indications. In this sample, the branch on the top right image is aligned with the indication at the bottom right image.

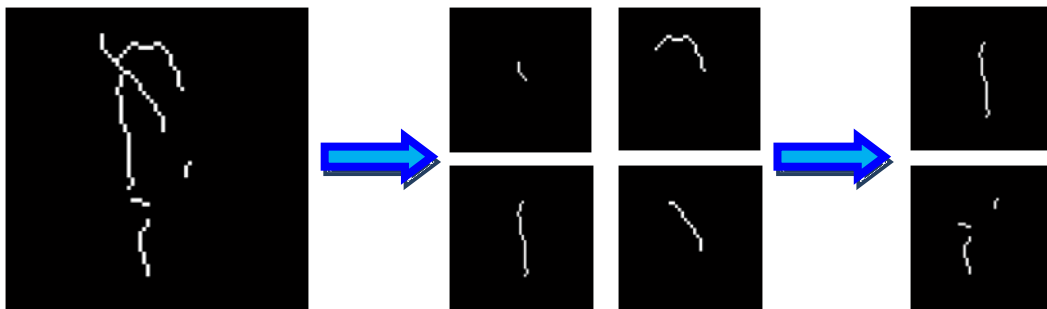


Figure 3.20 Aligned indication detection: a complex case which the indication has several branches

3.5 Software interface and results

In order to display the testing result and aid human inspector, a user friendly software interface is designed in this thesis to show image processing procedures and classification results (Figure. 10). The interface is developed in Matlab GUIDE.

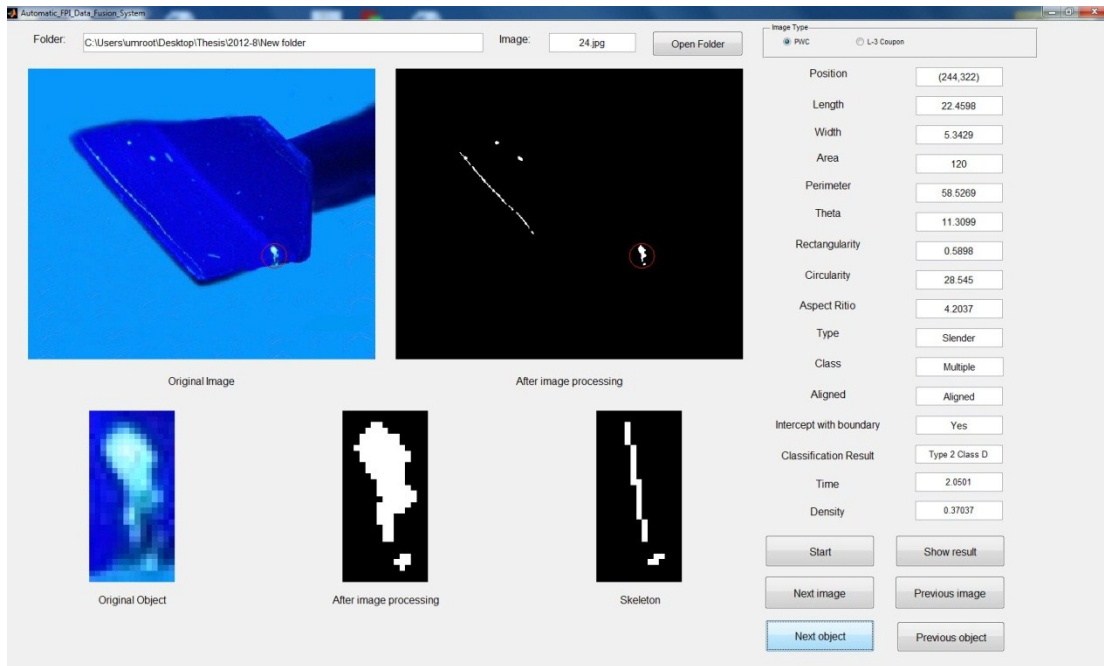


Figure 3.21 AAIS software interface built in MATLAB GUIDE

In the interface, we integrate all the functions and show the image processing, segmentation, feature extraction and classification results. On the left of the interface, the image results are shown step by step. On the top right part of the interface, the feature extraction results are displayed such as Center position, Length and Width, Area, Minimum enclosing rectangle, Aspect ratio, Perimeter and Rectangularity. The bottom right part shows the classification results. The interface can process all the images in a folder specified by user and obtain the classification result automatically. This well designed interface eases human inspector's work and gives visualized results in detection, classification and measurement.

As a result, in the 44 testing images provided from the industrial partner—Pratt-Whitney, 223 indications are correctly detected, 21 indications are not detected or

incorrectly detected. Among the correctly detected indications, 211 indications are correctly classified while 12 indications are incorrectly classified. The final detection rate is 91.4% and classification rate is 94.6%. The results are accepted by our industrial partners.

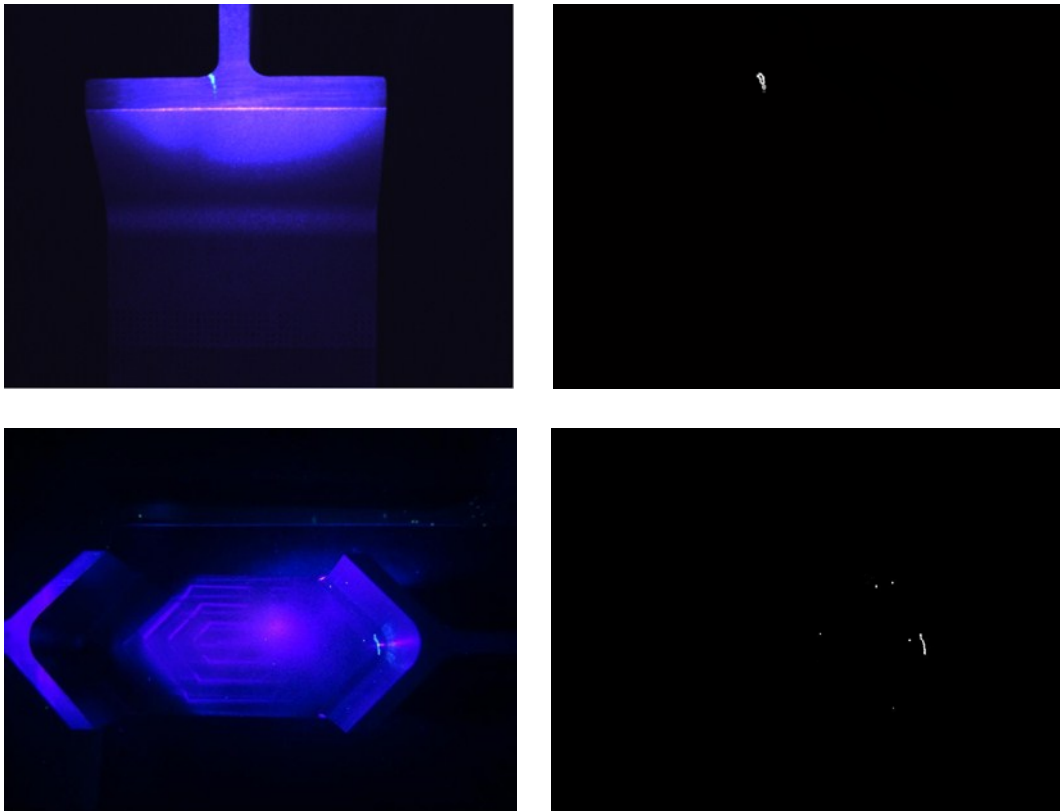


Figure 3.22 FPI tests on coupon samples

Field tests on coupons with the same material and similar size of defects have been taken as a demonstration of FPI testing and image processing and classification algorithm. There are 6 coupons and 4 cracks that are found by FPI tests and all of them are correctly classified by the algorithm. Samples and image processing results are shown in Figure 3.22.

3.6 Conclusion

In this chapter, we successfully designed an AAIS for Turbine Blade FPI analysis with high accuracy and efficiency. Image preprocessing functions are implemented to enhance green indications, smooth the image and reduce noise. Image segmentation functions combine morphological operations with Otsu adaptive threshold method and Canny edge detection to segment input image into background image, foreground image and indication bitmap image. Feature extraction functions are developed for the specific problem and classification function is developed to classify indications into 2 types and 4 classes according to ASTM-E433 Liquid Penetrant Inspection Standard. A software interface is designed to control and display the process. The system is tested by both sample images and FPI results from couple.

The test results demonstrate that the developed system can automatically detect indications from turbine blade FPI results, give accurate measurements and classification into 2 types and 4 classes according to ASTM-E433 standard. This system can aid human inspectors to perform FPI analysis effectively in measuring useful features and classifying indications.

Chapter 4. Image processing and classification applications in honey bee colony health monitoring

4.1 Introduction

In Canada, honey bee industry is an important part of this country's agricultural production, makes Canada the world's twelfth-largest producer of honey. According to recent research, Canadian bee keepers suffer from Colony Collapse Disorder (CCD) in the past few years. Over the winter of 2008-2009, Canadian bee keepers lost 33.9% of colonies, twice the normal rate of winter losses. In some provinces such as Alberta, New Brunswick and PEI, the number exceeds over 40%. Biologists and experts have proposed and examined numerous causes of this winter loss, until now we are sure that no single factor is the cause. Hence monitoring and detection of the diseases and the disorder is critical to prevent more loss and control the colony number. To prevent disease and identify unhealthy colony, the bee keepers work day by day to examine every colony, which costs a lot in terms of time and money. A much more effective and economic solution in bee colony monitoring is highly needed.

In North America, honey bees are always kept in brood boxes which normally contain 10 man-made frames (Figure 4.1). In each frame there are 2000 to 3000 empty cells to let bees build their colony. To inspect health condition in a colony, beekeepers will open up a brood box and take the frame to analyze. The frame in the middle always has the

biggest brood area since the whole brood is olive like in 3-D space. Beekeepers need to measure the brood area against the whole frame area and also the unhealthy (uncapped) cells against the healthy (capped) cells inside the brood area.



Figure 4.1 A brood box with 10 man-made frames

The brood area consists of bright color capped cells with uncapped cells. A healthy colony's brood area is big and the capped cells are the cells in the majority of the brood (Figure 4.2). The beekeepers will decide the brood area and measure the area with the traditional rules. Meanwhile they count the capped cells and uncapped cells in the brood area manually. Then they will calculate two percentages:

$$\frac{TBC}{TFC} \% = (Brood\ area)/(Total\ frame\ area) \quad (4.1)$$

$$\frac{BH}{TBC} \% = (Brood\ uncapped\ cells)/(Total\ brood\ cells) \quad (4.2)$$

Based on the above two percentage, they will make their decision by comparing those data

with empirical standards to detect the health condition.

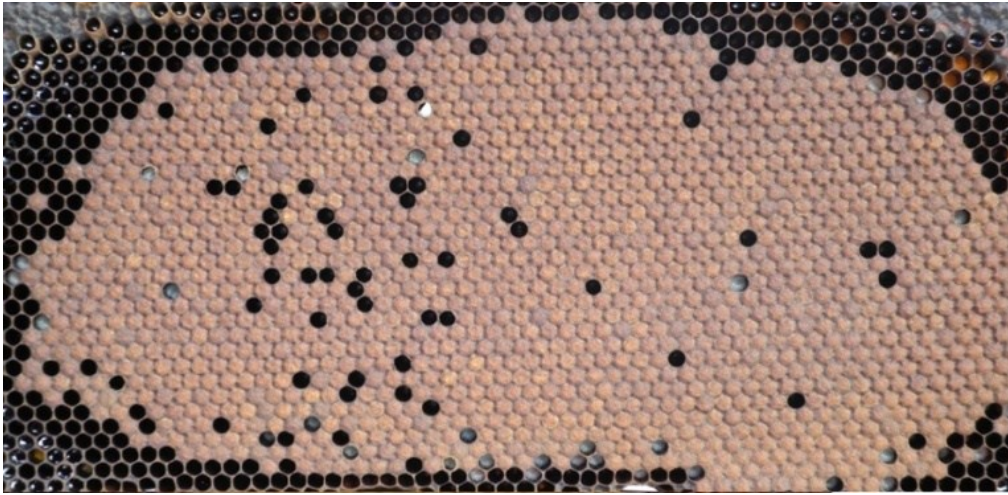


Figure 4.2 A healthy brood sample

This process is time and labor consuming. It normally takes 50 minutes to evaluate one brood, and there are hundreds and thousands brood boxes in a farm. That will take hundreds of hours to inspect a whole farm. By the way, human cannot make accurate inspection all the time especially after long working hours. In order to increase the speed and accuracy of the whole process, we collaborate with Novatek International to design an advanced bee colony health monitoring system which consists of hardware and software parts. In the hardware part, we set up an inspection box with cameras, where one can insert a brood frame and take picture in standard lighting and definition condition. In the software part, we have implemented automatic inspection function which includes extracting brood area, inspecting the uncapped cells inside the brood and making decision whether the brood is healthy or not. The images we have processed are provided by the industrial partner-- Novatek International, which stand for typical beehive health conditions under different

kinds of situations. However, the images are taken under non-uniform conditions. Hence, we may face different definition, contrast, lighting conditions, and sometimes there are bees in the image. To solve these problems, we have implemented different image processing techniques such as, gray scale image, noise reduction, adaptive threshold, morphological transform, curve fitting, and Hough transform. In the decision step, we implement artificial neural network to classify images and give the final decision.

In this chapter, we will introduce the hardware set up: inspection box with camera in section 4.2. In section 4.3, image preprocessing functions will be explained briefly. In section 4.4, the brood area will be segmented out of frame image using edge detection, curve fitting functions, adaptive thresholding and morphological operations. In section 4.5, feature extraction of circularity will be carried out with Hough transform circle detection to detect the uncapped cells in the brood area. In section 4.6, 6 images provided by our industrial partner will be tested, and the results will be presented.

4.2 Brood frame inspection box

As mentioned in the introduction, beekeepers need to take out a single frame and inspect health condition. In this project, we need to take pictures of each frame. To control the lighting of picture and guarantee all pictures will have unified high quality, we designed an inspection box (Figure 4.3). The box has a frame slot in the middle, two digital cameras at both sides with LED lightening sources. And the box is portable; it's easier for beekeepers and researchers to carry between farms and research centers. When inspecting a

frame, one can insert the frame into the slot and take pictures. This inspection box will ease beekeepers' work and ensure the quality of the pictures which is critical in the following image processing steps.

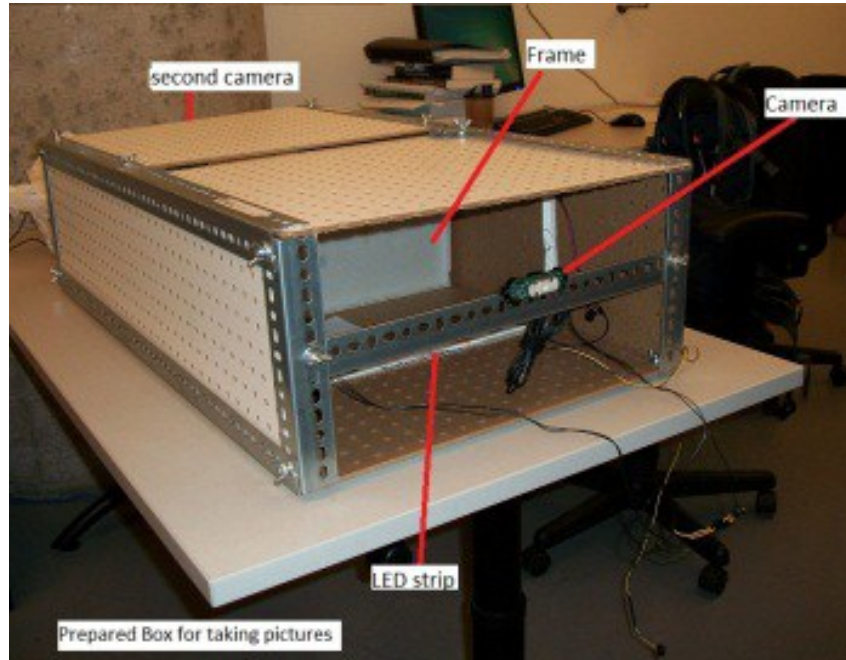


Figure 4.3 Inspection box with cameras

4.3 Image pre-processing

The sample images of brood colony which we use in this project stand for different situations, different lighting conditions, definitions, contrast and color. So the first step in the software design is to obtain gray scale images with good quality for further processing work. The pre-processing procedure contains three functions, i.e. 1. transforming RGB image into gray scale image, 2. noise reduction and 3. gray scale modification.

The sample images are standard RGB images, which is in a 3-D color space. Since

processing the image in RGB space is complex and time consuming, we need to transform the images into gray scale color space using Equation 2.4. Then we apply the similar procedure in Chapter 3, noise reduction functions.

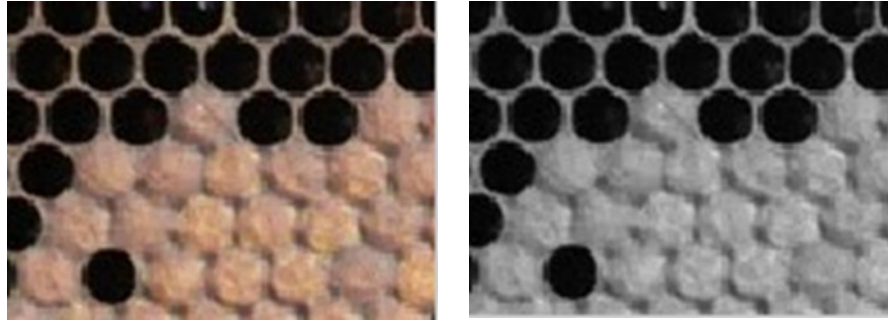


Figure 4.4 Convert a RGB brood frame image to standard gray scale image

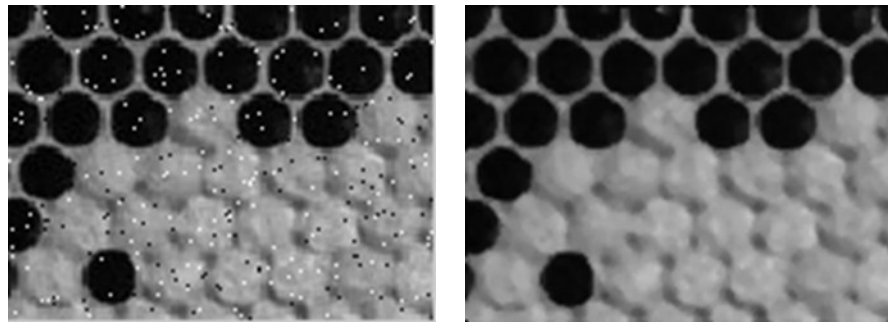


Figure 4.5 Noise reduction by Median filter with Wavelet approach

After we obtain the noise reduction result, contrast enhancement is necessary for enhancing the image. In this section we will implement histogram modification function. Compared with the other intensity transformation functions such as Gamma transform in section 3.3, histogram can improve contrast of poor contrast images. With good contrast, it is relatively easy to do further processing such as threshold or edge detection. The method will first draw histogram and mark the highest and lowest gray scale value of an image. Then it will extend the histogram to 0 to 255. Figure 4.6 shows an example of histogram modification.

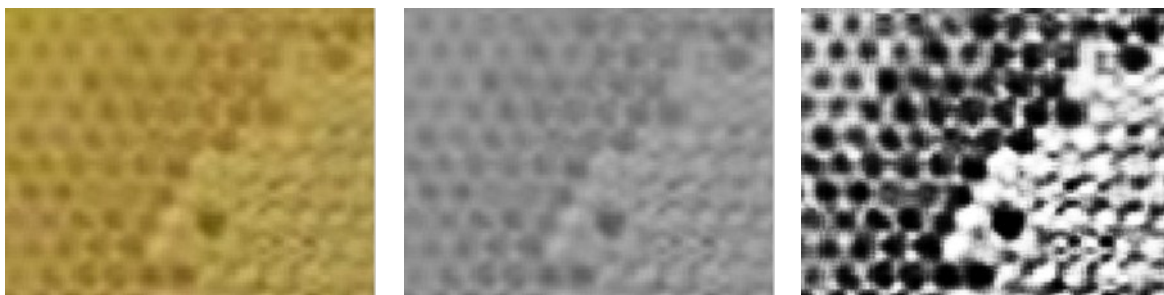


Figure 4.6 Original image, gray scale image and histogram modification result

4.4 Brood area detection

Brood area is the area where honey bees live. In brood frame images, brood area mainly contains healthy capped cells, unhealthy uncapped cells and bees or other objects under some circumstances. A beekeeper need to identify this area and count the number of capped cells and uncapped cells manually and calculate $\frac{TBC}{TFC}\%$ and $\frac{BH}{TBC}\%$ to evaluate the condition of one brood. In the developed system, we try to follow the same procedure in software by using image segmentation techniques. The first goal we need to reach is to detect brood area boundary automatically in software. We have tried different techniques to obtain the brood boundary, edge detection filtering, adaptive threshold and morphological transform. In some cases, it is hard to get a good boundary, so further we have applied the curve fitting functions to deal with this situation.

4.4.1 Edge filtering

Edge filtering is the most basic and popular way in edge detection. As mentioned in Chapter.3, Canny filter is a double threshold method and it has two thresholds and a sigma value to change the size of a Gaussian filter. The Gaussian filter will smooth the image at first, so we can change sigma to ignore the cells information and only consider the broad boundary. By modifying the sigma and two thresholds, we obtain the result as shown in Figure 4.7.

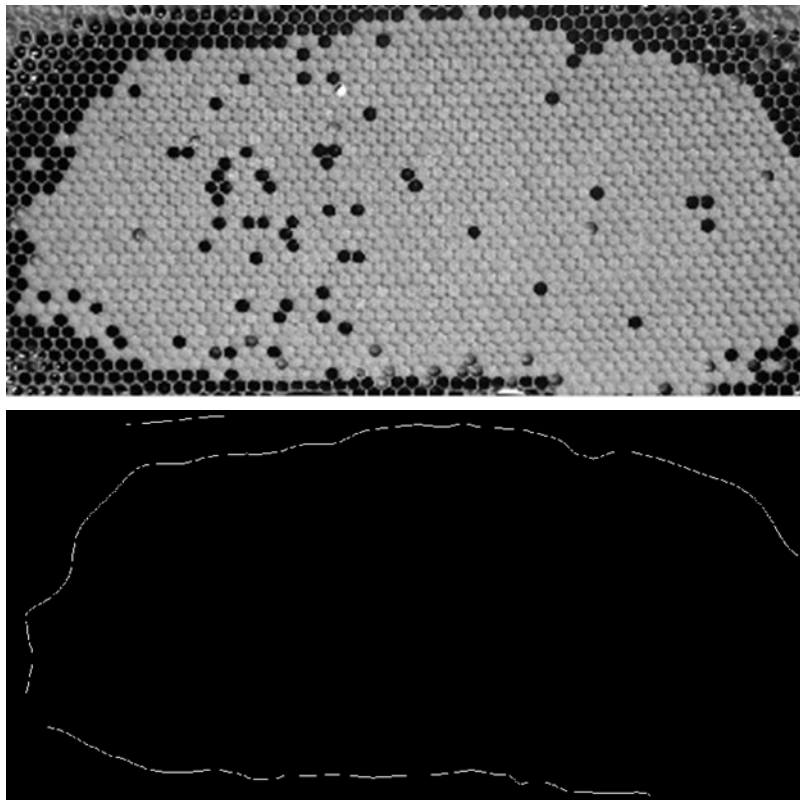


Figure 4.7 Canny edge detection result

Even though we have tuned those parameters by trial and error for many times, the result is still not very desirable. One reason is that we need an enclosed boundary in order to carry out the area calculation and further uncapped cell detection. In the result there are a lot of discontinuous boundaries. Some of them may be caused by the frame, which is

small and easy to connect. Others are caused by empty cells, 1 cell, 2 cells big or even bigger, and there may be some noise other than edge. It is impossible to find an easy way to connect these gaps, so we turn to an alternative solution: adaptive threshold with morphological transform approach.

4.4.2 Adaptive threshold with morphological transform

In order to get better results in brood boundary detection, we tried an alternative way. In the gray scale image, there is a difference in gray value between brood and frame, which enables thresholding to segment the brood. Here we use the Otsu adaptive thresholding method from Chapter.3 to perform thresholding to the gray scale brood image. Figure 4.8 shows the result after thresholding.

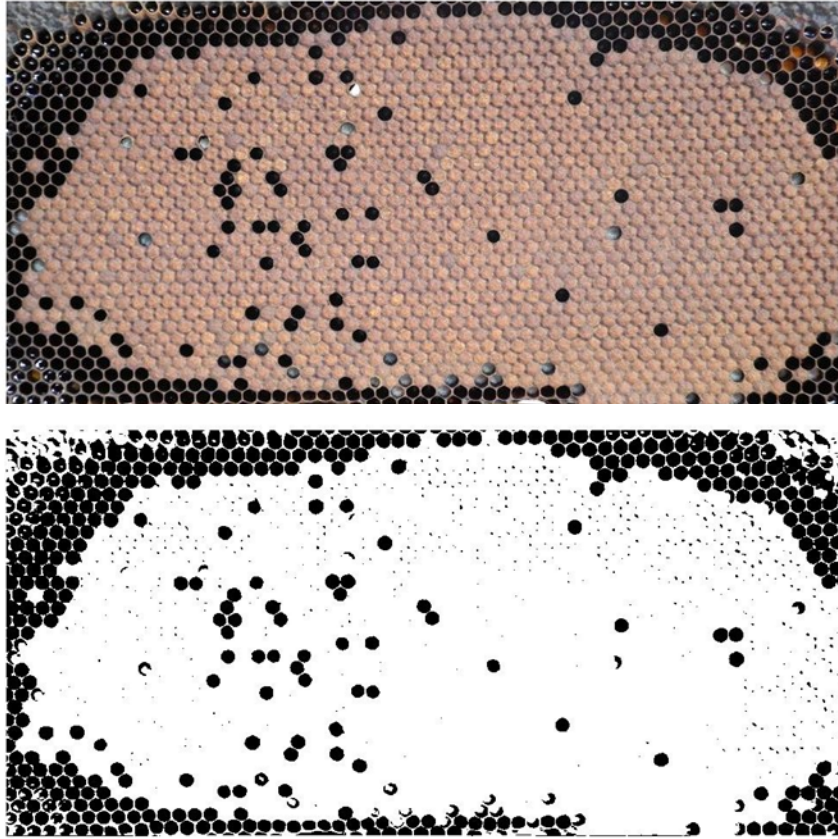


Figure 4.8 Otsu adaptive thresholding result

Form the result we can see there are small gaps caused by frame. We implement erosion function to thin the frame and reverse the image Figure 4.9.

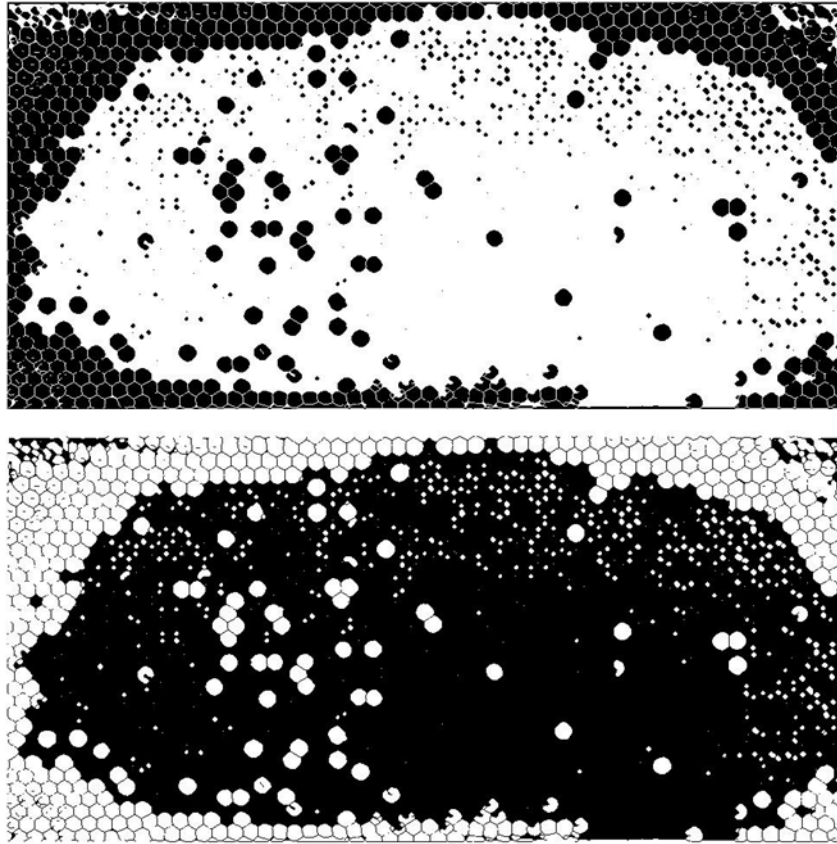


Figure 4.9 Image erosion and reverse result

Now the brood area is surrounded by white cells. We can implement dilation function to further eliminate gaps between cells. The brood area can be closed this way, then we can eliminate other cells and get the accurate brood boundary image. Figure 4.10 shows the process and result of boundary detection.

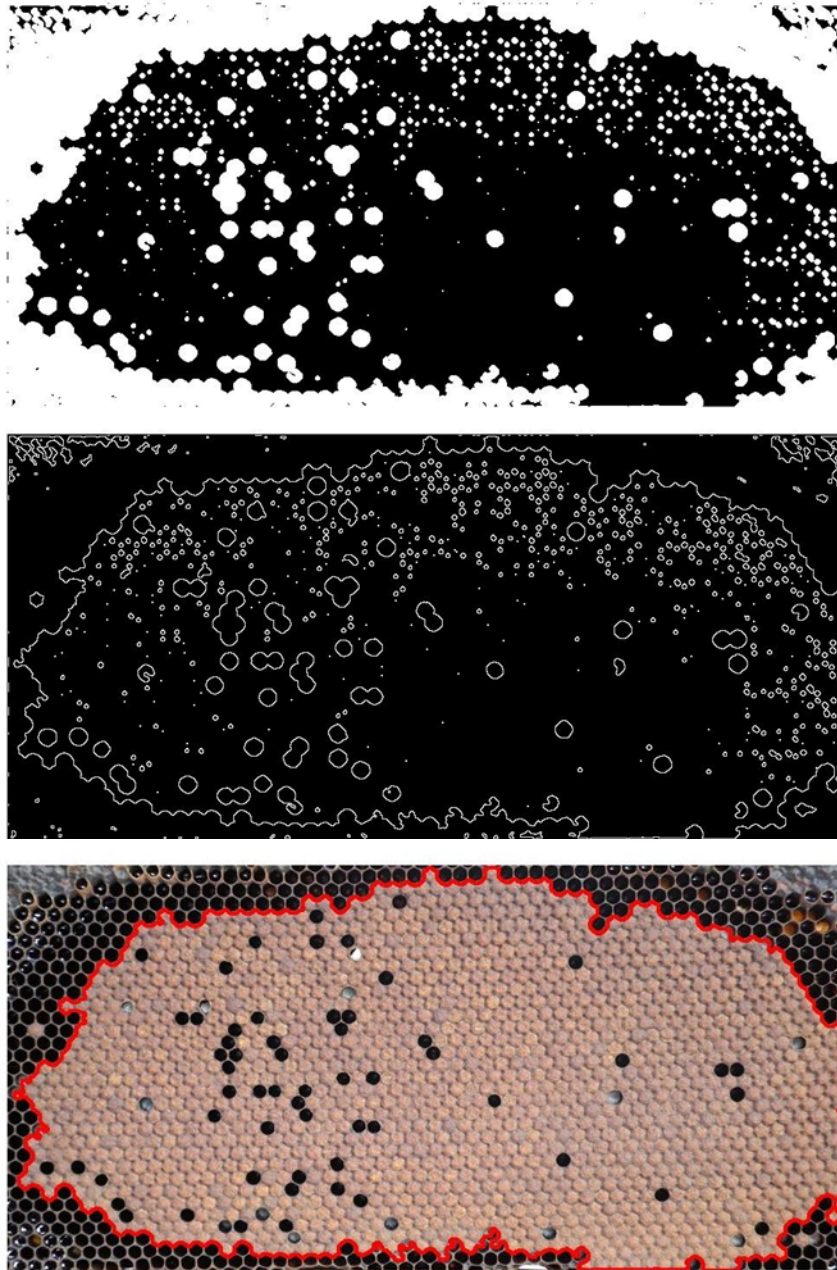


Figure 4.10 Result of brood boundary detection

In some cases, boundary detection may be interrupted by uncapped cells. In Figure 4.11, the detection result in red is incorrect, and the boundary at the bottom of this brood should be near the blue line. The boundary is blocked by empty cells in green. Since the

brood area is always similar to ellipse shape, we fit the detect boundary to an ellipse and use this ellipse to replace the incorrect part of the boundary. The result still has some errors, but it has been improved significantly and can be accepted for brood area detection.

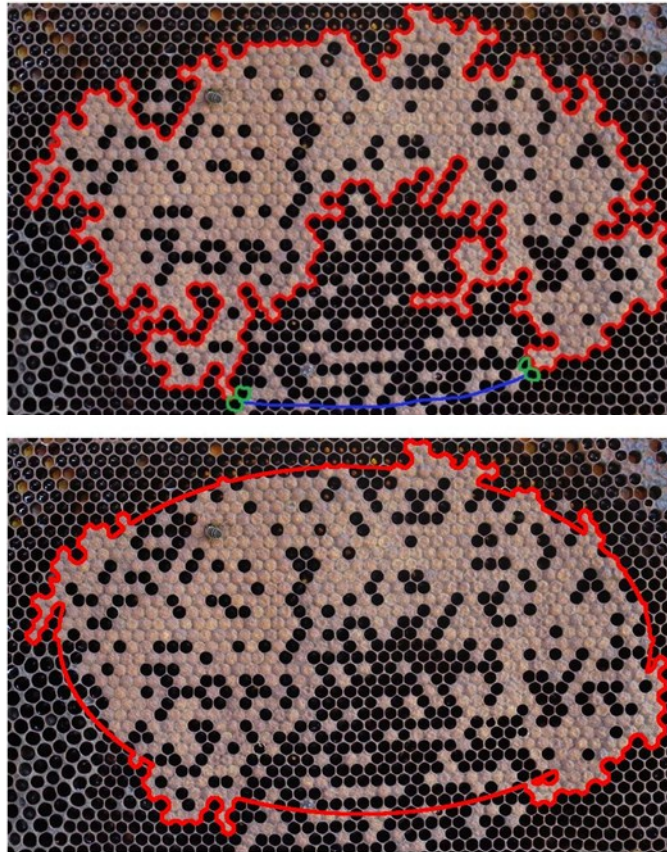


Figure 4.11 Result of ellipse fitting function

As a result, we successfully obtained accurate brood boundary information from input frame image. We can calculate $\frac{TBC}{TFC} \%$ from the brood area from the result. This value gives a general idea of how well is one brood grows in early development stage.

4.5 Brood area detection

The uncapped cell is the empty cell in the brood and it is an important evidence to tell if a brood is healthy or not. In the field testing, beekeepers will count the number of uncapped cells and compare this number with total brood cell number. In the developed algorithm, after we have detected the brood boundary, we process the brood image again using Otsu adaptive thresholding method to get the information inside brood.

After we detect and label all the objects inside brood and measure the features such as area, perimeter and boundary pixels, we can find that there are mainly three kinds of objects remaining in the brood: the circular objects which has the area around the average cell area representing the uncapped cell; some arc or fan-shaped objects also representing the uncapped cells; the noise object caused by bees and frame. The object caused by the bee is large and shapeless, and the object caused by frame is very tiny. We need to analyze the shape of an object to distinguish between uncapped cells and noises. Figure 4.12 shows all three kinds of object in brood area.

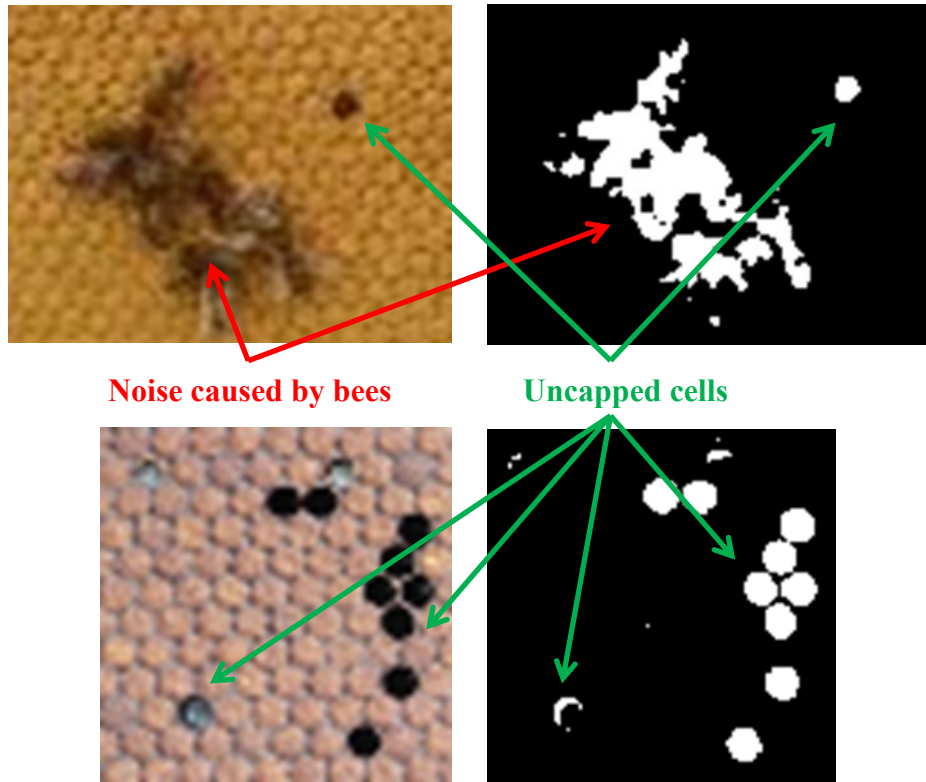


Figure 4.12 Circular uncapped cells, noises and Arc or fan-shaped uncapped cells

4.5.1 Circular uncapped cells detection

Unlike the other two kinds of object in the brood area, circular uncapped cells are in specific shape and area, which are easier to be detected. There is a very useful feature to detect circular objects: circularity.

For the circular uncapped cell detection, we measure the circularity in the objects which has the area over 80% of the average. Circularity is a parameter which roughly describes the shape of an object.

$$C = P^2 / A \quad (4.3)$$

where P is the perimeter of the object, A is the area of the object. Circularity takes on a

minimum value of 4π if the object is a circle. The shape of an object becomes more complex with bigger circularity value. In this way, we can easily detect the circular uncapped cells among the noises and arc objects (Figure 4.13).

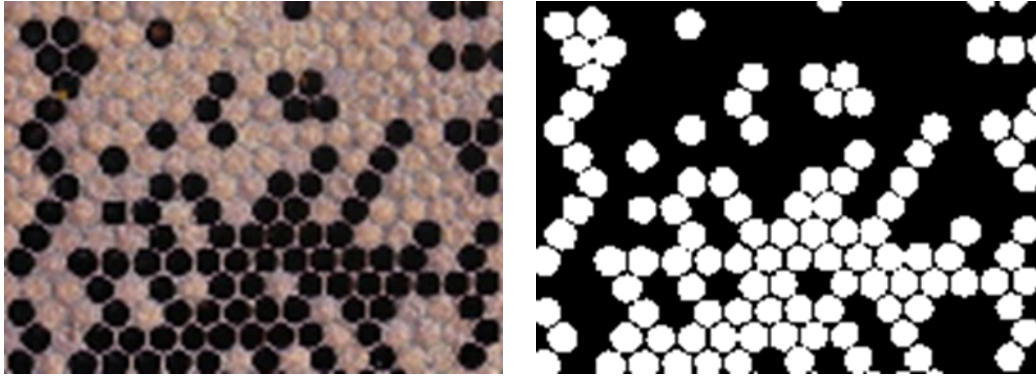


Figure 4.13 Circular uncapped cells detection

4.5.2 Arc or fan-shaped uncapped cell detection

To detect the arc or fan-shaped uncapped cell, we could not judge from its circularity value since the shape is complex. Here we refer to Hough transform which we implemented in Chapter.3 in line detection. In this section we will use Hough transform to detect arc and fan-shape.

Hough transform has the ability to detect many kinds of shapes. It means that if we know the equation of a certain pattern, and are able to transform the image into this particular parameter space, we are able to detect this certain pattern in Hough transform. For the arc and fan-like shape, we transform the image into a 3-D parameter space $a-b-r$ space (Equation 4.4), where (a, b) is the center point of circle and r is the radius of circle.

The algorithm will scan every point in the input image as center point (a, b) , and at this point certain range of r . Then it will set step and range θ and scan the points around the center (a, b) with radius r to detect the arc. In this way, we are able to detect arc and fan that have the radius around the average cell radius. (Figure 4.14)

$$\begin{cases} a = x - r * \cos\theta \\ b = y - r * \sin\theta \end{cases} \quad (4.4)$$



Figure 4.14 Hough transform detect the arc or fan like uncapped cells

As a result, the algorithm successfully detects all uncapped cells inside the brood area. Then it can calculate another important percentage value: $\frac{BH}{TBC}$ %. With the results from Section 4.4, we can proceed to decision making step in the next section.

4.6 Artificial Neural Network decision making

In the previous sections, we successfully detect the boundary of brood and uncapped cells, we can make decision according to $\frac{TBC}{TFC}$ % and $\frac{BH}{TBC}$ % mentioned in Section 4.1. In the field testing, the beekeepers will compare $\frac{TBC}{TFC}$ % and $\frac{BH}{TBC}$ % with the brood

growth empirical data to decide the status of the brood. In the software, we implement artificial neural network to increase accuracy and robustness of the final decision making. ANN is a widely used tool in pattern recognition and it is easy to be trained and used as classifier (Section 2.7). In this project, we use $\frac{BC}{TFC}$ % and $\frac{BH}{TBC}$ % as the input of the ANN, and train the ANN by Back-Propagation training method (BP). The trained ANN can be used for health condition detection. Then we implement this ANN into our software to make the final decision.

4.7 Software interface and test result

A software interface is developed in this thesis to show all the procedures and the processing result (Figure 4.15). The interface is developed in Matlab GUIDE. The top left of the interface shows the brood boundary detection result. The top right area shows the re-processing result inside brood area and the bottom one shows the final result of uncapped cells detection. The detection results include brood area, brood cell number, average area of cells, $\frac{TBC}{TFC}$ %, uncapped cell number, $\frac{BH}{TBC}$ % and evaluation decision. The interface will process all the images in a specified folder and display the results automatically within a few seconds.

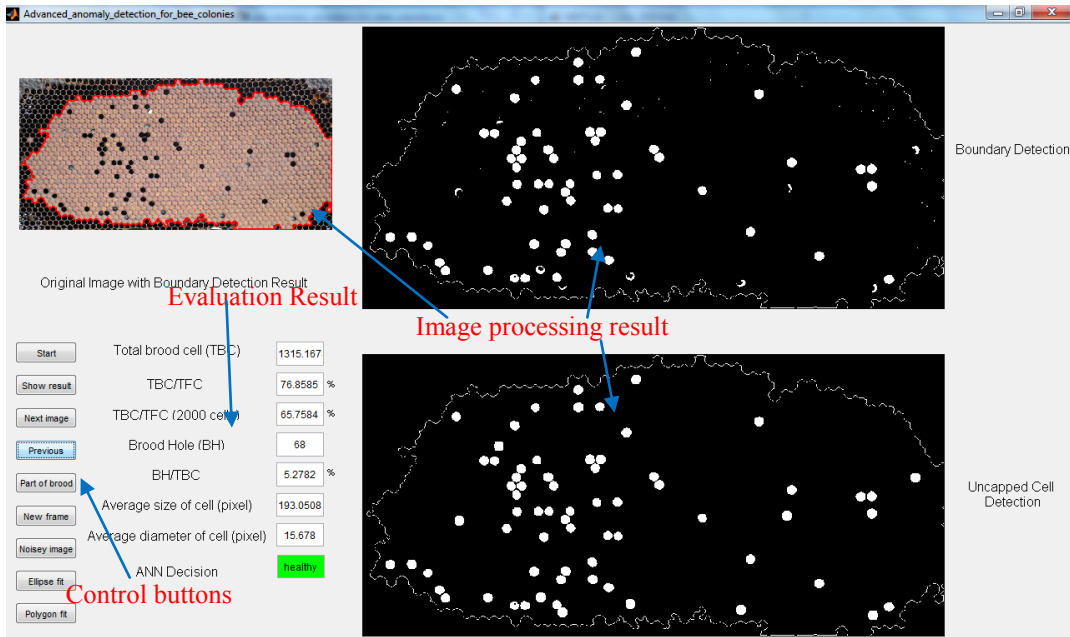


Figure 4.15 Software interface

To test the system's capability and robustness, 6 pictures standing for typical cases in the field work have been processed. Figures 4.16 to 4.21 show the testing results for those sample pictures.

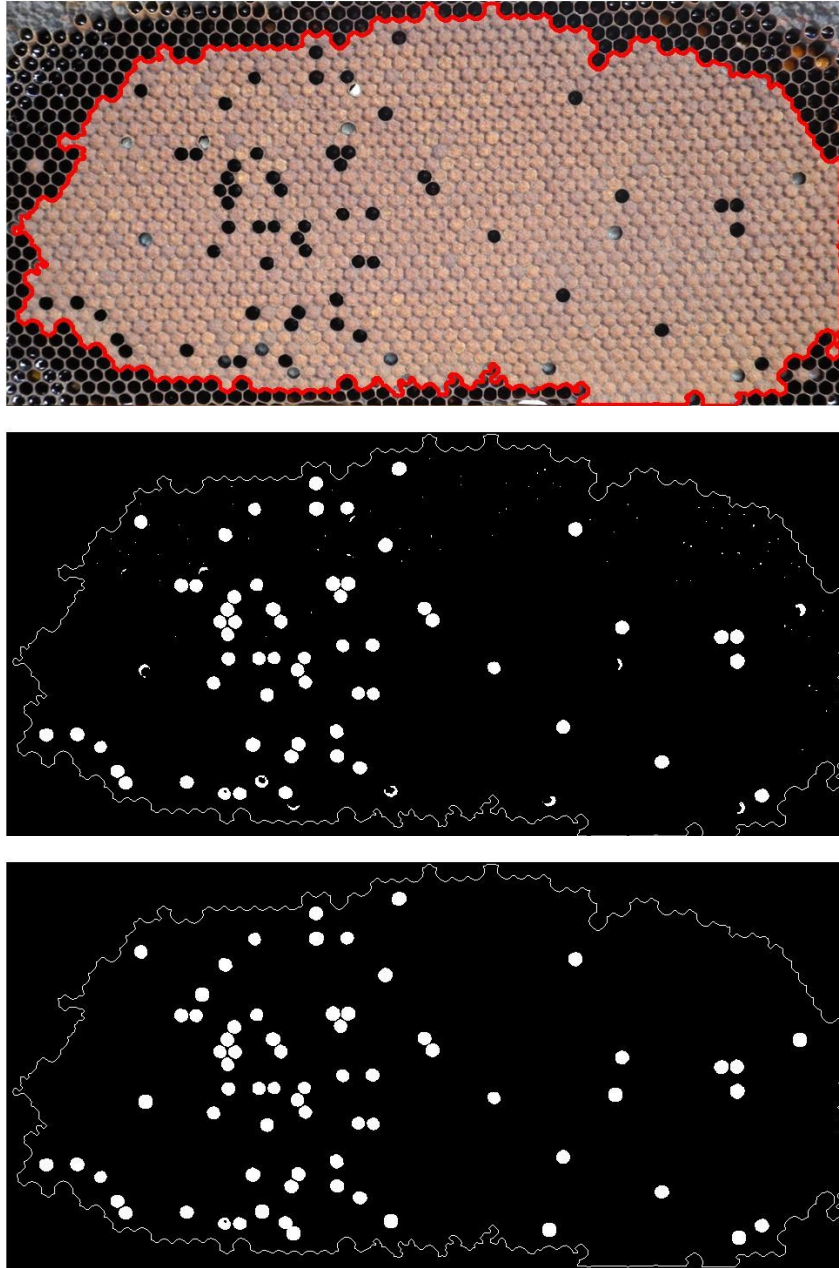


Figure 4.16 Result of picture 1: Arc or fan-shaped uncapped cell detection

In Figure 4.16, the brood area detection is accurate. Inside the brood area, some small noises caused by frame have been removed, and Arc or fan-shaped uncapped cells are detected by the system. $\frac{TBC}{TFC}$ % is 76.85% and $\frac{BH}{TBC}$ % is 5.28%, the final decision is

healthy.

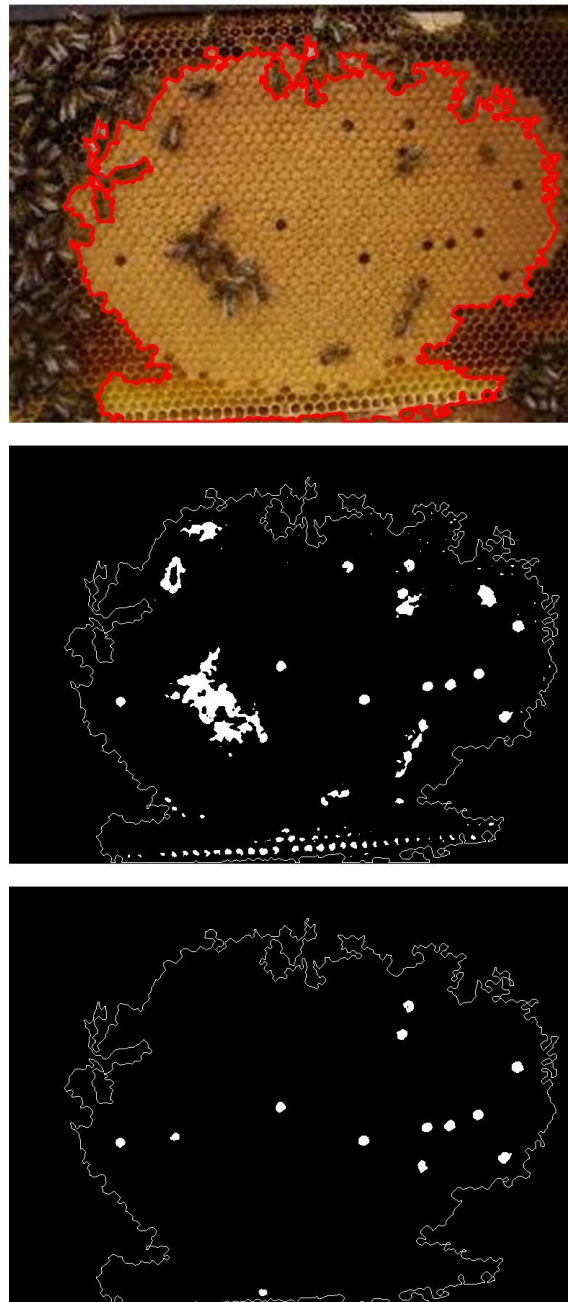


Figure 4.17 Result of picture 2: big noises from bees

In Figure 4.17, the big noises caused by bees staying on the brood frame have been eliminated by the system. $\frac{TBC}{TFC}$ % is 57.46% and $\frac{BH}{TBC}$ % is 1.07%, the final decision is

healthy.

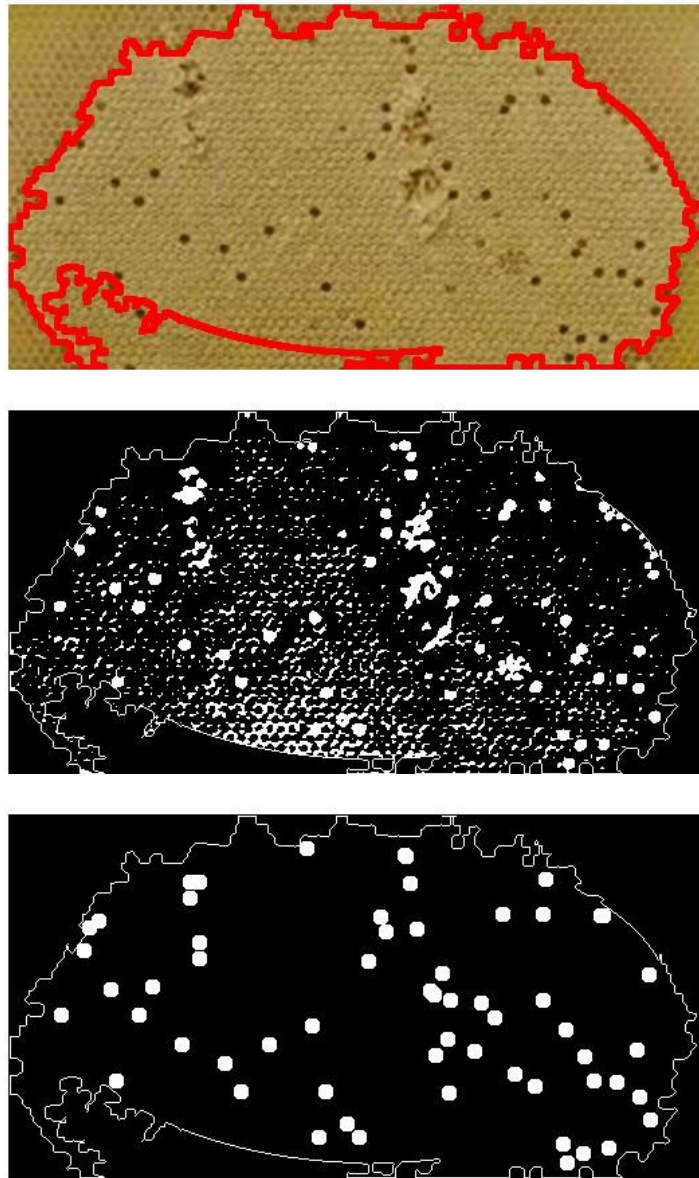


Figure 4.18 Result of picture 3: low contrast and definition

In Figure 4.18, the picture's contrast and definition are very low. That brings a lot of noise to the result. Brood boundary detection needs assistance from the ellipse fitting

function. $\frac{TBC}{TFC}$ % is 72.78% and $\frac{BH}{TBC}$ % is 8.20%, the final decision is healthy.

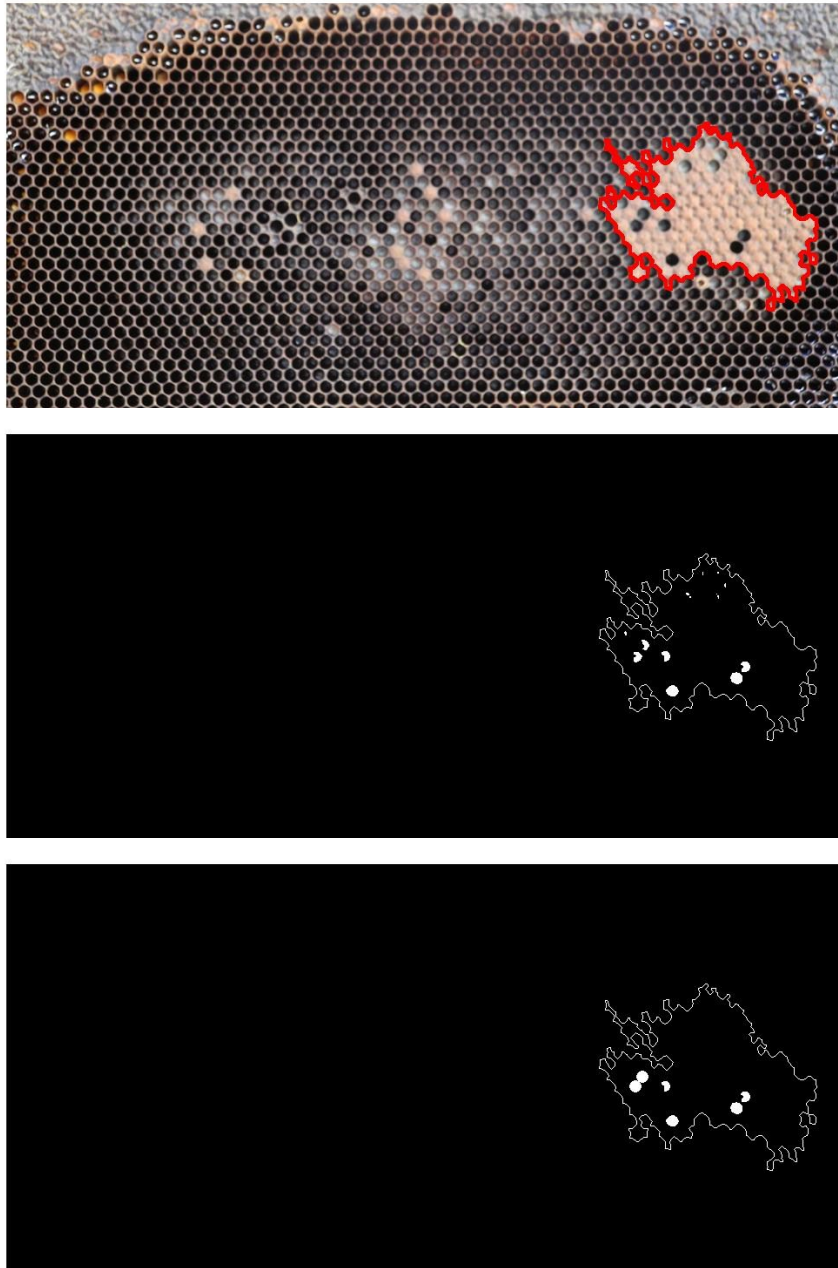


Figure 4.19 Result of picture 4: Arc or fan-shaped uncapped cell detection

In Figure 4.19, the brood area is very small compared with the whole frame. $\frac{TBC}{TFC}$ %

is 6.17% and $\frac{BH}{TBC}$ % is 3.77%, the final decision is unhealthy.

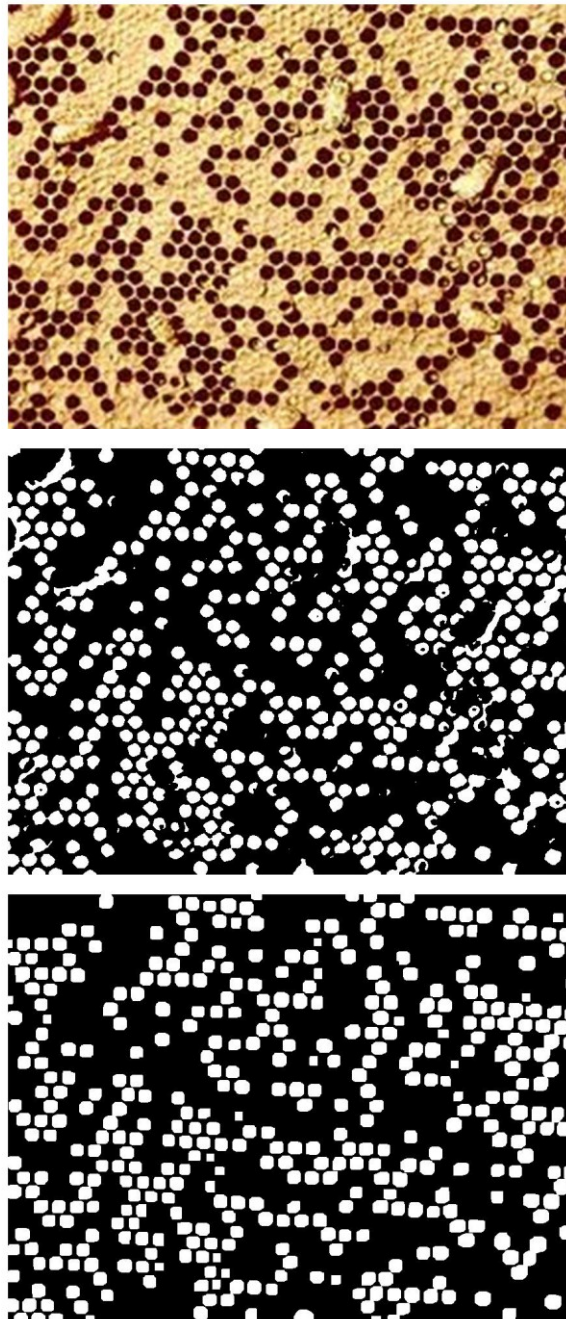


Figure 4.20 Result of picture 5: unhealthy brood with large number of uncapped cells

In Figure 4.20, there are large numbers of uncapped cells inside the brood area.

$\frac{BH}{TBC}$ % is 38.79%, the final decision is unhealthy.

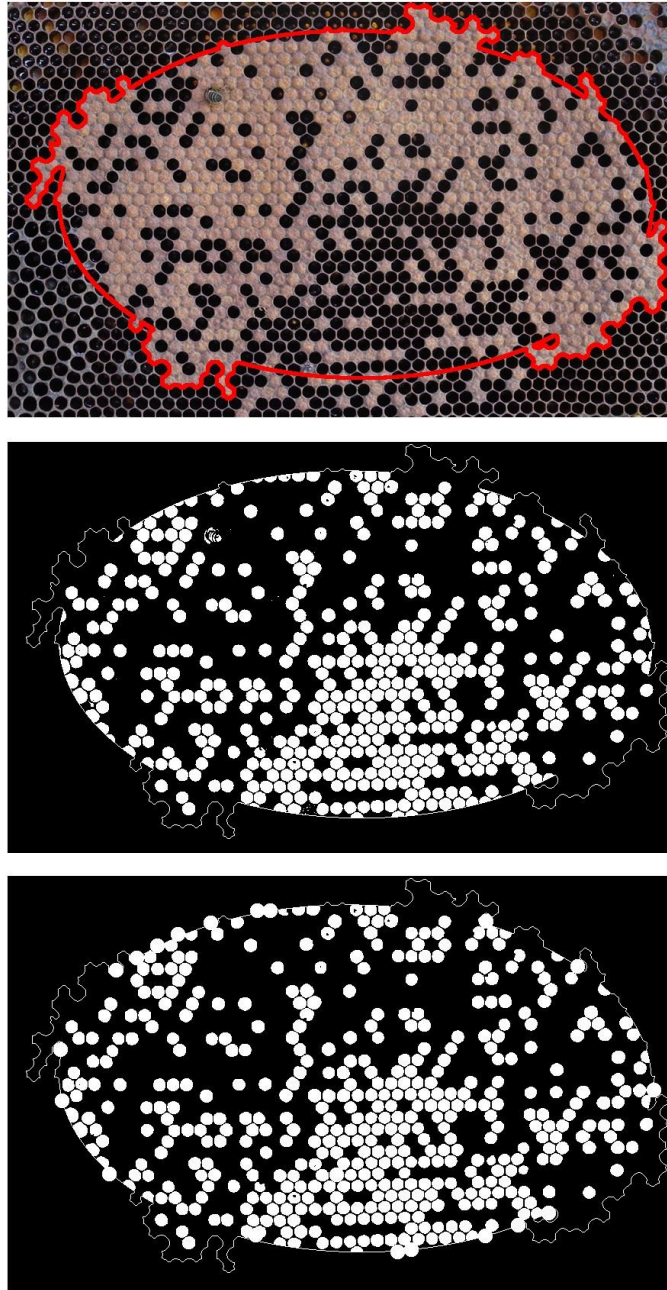


Figure 4.21 Result of picture 6: brood boundary interrupted by uncapped cells

In Figure 4.21, the brood boundary is interrupted by uncapped cells, and the brood area detection is assisted by ellipse fitting function. Inside the brood area, large numbers of

uncapped cells are detected. $\frac{TBC}{TFC}$ % is 63.27% and $\frac{BH}{TBC}$ % is 44.89%, the final decision is unhealthy.

Table 4.1 shows the software results compared with the manual counting results. From image 1 to image 6 we can see our software successfully detect the brood boundary and uncapped cells inside the brood. We can see we have precise $\frac{TBC}{TFC}$ % and $\frac{BH}{TBC}$ % in image No.1, No.2 and No. 6. In image No.4, the 5 uncapped cells near the upper boundary are too bright to be detected by the software and hence the software gives some errors in detection. In image No.3 and No.5, the error is caused by the big definition difference from other images. However, due to universal approximation and robustness of ANN, the final decisions made by ANN are all correct.

Table 4.1 The TBC/TFC and BH/TBC percentage counted using the developed software and manually

No.	Manually				Software			
	TBC/TF C %	BH/TBC %	BH	Decision	TBC/TF C %	BH/TBC %	BH	Decision
1	69.80	5.78	75	healthy	76.85	5.28	68	healthy
2	64.00	0.97	13	healthy	57.46	1.07	13	healthy
3	84.00	3.52	61	healthy	72.78	8.20	60	healthy
4	6.40	9.09	9	unhealthy	6.17	3.77	6	unhealthy
5	NaN	52.02	489	unhealthy	NaN	38.79	431	unhealthy
6	57.00	41.30	471	unhealthy	63.27	44.89	458	unhealthy

4.8 Conclusion

In this chapter, we successfully developed an advanced bee colony health detection system to improve the efficiency of bee colony health evaluation with high accuracy. Our system successfully evaluated 6 sample image selected by industrial partners. A series image processing and edge detection algorithms have been implemented for image pre-processing, brood boundary detection and uncapped cell detection tasks. A software interface has been developed to demonstrate each step and a neural network has been trained to classify the health condition of beehive automatically. The system is very practically designed and it provides a solution for beekeepers to replace the time and labour consuming manual inspection in the bee farms.

Chapter 5. Conclusion

5.1 Summarize of research work

In this thesis, image processing and classification techniques have been reviewed. Two research projects have been successfully carried out to solve two different practical detection problems which use image processing and classification techniques to detect the conditions of turbine blades or honey bee.

In the design of an advanced automatic inspection system for turbine blade FPI analysis, the research work is summarized as follows:

- A new approach combining Otsu Adaptive Thresholding with Canny Edge Detection and Erosion — Dilation – Subtraction method is developed to perform automatic accurate segmentation of turbine blade indication from background after FPI process.
- Some novel feature extraction and classification functions are designed to perform automatic classification of indications.
- A user friendly interface is designed to show detection and classification results of the advanced automatic inspection system for turbine blade FPI analysis.

In the design of an advanced automatic inspection system for honey bee colony health monitoring, the research work is summarized as follows:

- A new simple and effective approach integrating Otsu Adaptive Thresholding

and morphological operations is developed to perform automatic brood boundary detection with high accuracy.

- A new approach to uncapped cells detection is developed by integrating circularity detection and Hough circle detection.
- A user friendly interface is designed to show detection and classification results of the advanced automatic inspection system for honey bee colony health monitoring.

5.2 Future work

The following research work can be investigated in the future:

- The results of the advanced automatic inspection system for turbine blade FPI analysis can be combined with the other NDT methods such as ECT and UT. FPI can only detect surface discontinuities and could not provide any interior information about the discontinuities. Compared with FPT, the processes of ECT and UT take more time but they are more accurate and can provide more information such as the depth of the crack etc. The introduction of these methods to the system is expected to increase the system's accuracy and robustness.
- There are around 1000 bee brood boxes in every farm, mobile devices like GPS and Cell phones can be integrated with the inspection system for honey bee health monitoring system to record the location of brood box and growth information of

honey bees, and the data can be sent to the bee research centers which are far away from farms for growth analysis and health monitoring purpose. This new system will bring the easiness and efficiency of disease control to a whole farm or even region of farms across Canada.

- The results from the inspection system for honey bee health monitoring are only tested with 6 images from industrial partners. In the future we could carry out field work with our inspection box to take more pictures with higher quality to tune our system.

References

- [1] P. J. Shull, *Nondestructive Evaluation: Theory, Techniques and Applications*. Marcel Dekker, INC, New York, 2001.
- [2] C. Hellier, *Handbook of Non-Destructive Evaluation*. McGraw-Hill, 2001.
- [3] R. C. Gonzalez and R. E. Woods, *Digital Image Processing, Third Edition*. Prentice Hall, Aug. 2007.
- [4] R. Splinter and K. Najarian, *Biomedical Signal and Image Processing, Second Edition*. CRC Press, May. 2012.
- [5] Nobuyuki Otsu, “A threshold selection method from gray-level histograms,” *IEEE Trans. Sys., Man.,* vol. 9, no. 1, pp. 62–66, 1979.
- [6] C.M.Bishop, *Neural Networks for Pattern Recognition*. Oxford University Press, 1995.
- [7] B. Li, Y. Shen and W. Hu, “Casting defects induced fatigue damage in aircraft frames of ZL205A aluminum alloy – A failure analysis,” *Materials and Design*, vol. 32, issue 5, pp. 2570–2582, May 2005.
- [8] Y. Bombardier, M. Liao, R.J. Hiscocks, R.S. Rutledge and D.S. Backman, “Damage tolerance analysis of the North American SNJ-6 wing lower attachment angle,” *Canadian Aeronautics and Space Journal*, vol. 56, no. 1, pp. 31-41, 2010.
- [9] J. Kunz, O. Kováík, H. Lauschmann, J Siegl and P Augustin, “Fractographic

- reconstitution of fatigue crack growth in integrally stiffened panels,” *Procedia Engineering*, vol. 2, issue 1, pp. 1711–1720, April 2010.
- [10] S. Soni and A. Chattopadhyay, “Sensitivity studies on sensor selection for crack growth investigation”, *Smart Mater. Struct.*, vol. 19, no. 105015, 2010.
- [11] G. Harvey and J. Jones, “Small turbine blade inspection using laser strain techniques,” *Insight Non-Destructive Testing and Condition Monitoring*, vol. 51, no. 3, pp. 137-139, Mar. 2009.
- [12] C. Bonavolontà, M. Valentino, G. Peluso, and A. Barone, “Non destructive evaluation of advanced composite materials for aerospace application using HTS,” *IEEE Transactions on Applied Superconductivity*, vol. 17, no. 2, pp. 772-775 June 2007.
- [13] G.F Harrison, “An overview of PEP WG28 - Recommended practices for monitoring gas turbine engine life consumption,” presented at Exploitation of Structural Loads/Health Data for Reduced Life Cycle Costs Meeting, Brussels, Belgium, 11-12 May 1998.
- [14] A. Jameel, “Surface damage tolerance analysis of a gas turbine engine rotor,” *Proceedings of the ASME Turbo Expo*, vol. 4, pp. 457-462, 2005.
- [15] B.W. Lee, J. Suh, H. Lee and T. Kim, “Investigations on fretting fatigue in aircraft engine compressor blade,” *Engineering Failure Analysis*, vol. 18, issue 7, pp. 1900–1908, Oct. 2011.
- [16] M-H, Cyrus B., “Detect, troubleshoot gas-turbine blade failures,” *Power*, vol. 139,

- no. 12, pp. 35-38, Dec 1995.
- [17] A. Rybnikov, L. Getsov and S. Leontiev, "Failure analysis of gas turbine blades," *Microscopy and Microanalysis*, vol. 11, no. 2, pp. 222-223, 2005.
- [18] M. T. Naeem, S. A. Jazayeri and N. Rezamahdi, "Failure analysis of gas turbine blades," in *Proceedings of the IAJC-IJME International Conference*, 2008, pp. 120-131.
- [19] M. Naeem, R. Singh, D. Probert, "Implications of engine deterioration for a high-pressure turbineblade's low-cycle fatigue (LCF) life-consumption," *International Journal of Fatigue*, vol. 21, no. 8, pp. 831-847, 1999.
- [20] R. Viswanathan, "An investigation of blade failures in combustion turbines," *Engineering Failure Analysis*, vol. 8, no. 8, pp. 493-511, 2001.
- [21] "Introduction to Nondestructive Testing", www.ndt-ed.org.
- [22] Kamal H.Dhandha, A.D.Bhathena, Manas Ghosh, and Dr.Sanjay Soman, "Study and comparison of different fabrication and NDT requirements for pressure vessel, boiler, piping, structure & nuclear component manufacturing with respect to various codes & standards," in *Proceedings of the National Seminar & Exhibition on Non-Destructive Evaluation 2011*, Dec. 2011, pp. 387-392.
- [23] C. Imbert and K. Rampersad, "Magnetic particle testing of turbine blades mounted on the turbine rotor shaft," *Journal of Testing and Evaluation (JTE)*, vol. 20, no. 4, July 1992.
- [24] V. V. Vakhov, I. B. Veretennikov, and V. A. P'yankov, "Automated ultrasonic testing

- of billets for gas-turbine engine shafts,” *Russian Journal of Nondestructive Testing*, vol. 41, no. 3, pp. 158–160, 2005.
- [25] E. Jasiūnienė, R. Raišutis, R. Šliteris, A. Voleišis, M. Jakas, “Ultrasonic NDT of wind turbine blades using contact pulse-echo immersion testing with moving water container,” *ULTRAGARSAS (ULTRASOUND)*, vol. 63, no. 3, pp. 28-32, 2008.
- [26] P. I. Beda and V. M. Sapunov, “Experience in eddy-current testing of mounting holes in aircraft components,” *Russian Journal of Nondestructive Testing*, vol. 36, no. 4, pp. 241-245, 2000.
- [27] R.O. McCary and J.R.M. Viertle, "Automating an eddy current test system for in-service inspection of turbine/generator rotor bores," *IEEE Transactions on Magnetics*, vol. 24, no. 6, pp. 2594-2596, Nov 1988.
- [28] Y.H. Wu and C.C. Hsiao, “Reliability assessment of automated eddy current system for turbine blades,” *Insight-Non-Destructive Testing and Condition Monitoring*, vol. 45, num. 5, pp. 332-336(5), May 2003.
- [29] J. L. Fisher, S. N. Rowland, J. S. Stolte and C. Salkowski, “Automated eddy current inspection of Space Shuttle APU turbine wheel blades,” in *Proceedings of the 17th Annual Review of Progress in Quantitative Nondestructive Evaluation*, La Jolla, CA., July 15-20, 1990, pp. 11-38.
- [30] “NDT Method Summary”, www.ndt-ed.org.
- [31] “Overview of Nondestructive Testing”, NDT: Guide to Non-destructive Testing, <http://www.asminternational.org>.
- [32] T.L. Adair, D.H. Wehener, M.G. Kindrew and H.I. Winter, “Automated fluorescent

- penetrant inspection (FPI) system is triple A,” in *1998 IEEE AUTOTESTCON Proceedings, IEEE Systems Readiness Technology Conference*, 1998, pp.498-529.
- [33] “Automatic FPI Ssystem: Large Batch Flow Type,” http://www.cyclo-system.com.sg/products/C54/automatic_fpi_system.aspx.
- [34] M. S. Kaseko, “A neural network-based methodology for pavement crack detection and classification,” *Transportation Research Part C: Emerging Technologies*, vol. 1, no. 4, pp. 275-291, Dec. 1993.
- [35] S. Nashat, A. Abdullah and M.Z. Abdullah, “A robust crack detection method for non-uniform distributions of coloured and textured image,” in *IEEE International Conference on Imaging Systems and Techniques*, May 2011, pp.98-103.
- [36] Y. Tian, D. Du, G.R. Cai, L. Wang and H. Zhang, “Automatic defect detection in X-Ray images using image data fusion,” *Tsinghua Science and Technology*, vol. 11, no. 6, pp. 720-724, Dec. 2006.
- [37] H.I. Shafck, E.S. Gadelmawla, A.A. Abdel-Shafy and I.M. Elewa, “Automatic inspection of gas pipeline welding defects using an expert vision system,” *NDT&E International*, vol. 37, no. 4, pp. 301-307, 2004.
- [38] G. Li, L. Min and H. Zang, “Color edge detections based on cellular neural network,” *International Journal of Bifurcation and Chaos*, vol. 18, no. 4, pp. 1231 - 1242, 2008.
- [39] H. Mu, L. Li, L. Yu, M. Zhang and D. Qi, “Detection and classification of wood defects by ANN,” in *Proceedings of the 2006 IEEE International Conference on*

- Mechatronics and Automation*, Jun. 2006, pp. 2235-2240.
- [40] Y.L. Luo, P.S. Qu and W.H. Dong, "Fault diagnose of aero engine based on digital image processing," in *Control and Decision Conference*, 2008, pp.3572-3575.
- [41] G. Weng, "Image processing and classification of metal fracture surface," in *Proceedings of the 2008 International Conference on Wavelet Analysis and Pattern Recognition*, Hong Kong, Aug. 2008, pp. 163-167.
- [42] Q. G and M. L. Jing, "Image-processing Algorithms of Magneto-Optic Imaging for Aircraft Multi-skin Inspection," in *2010 International Conference on Multimedia Technology (ICMT)*, 2010, pp.1-5.
- [43] J. Carroll, C. Efstathiou, J. Lambros, H. Sehitoglu, B. Hauber, S. Spottswood and R. Chona, "Investigation of fatigue crack closure using multiscale image correlation experiments," *Engineering Fracture Mechanics*, vol. 76, no. 15, pp. 2384 - 2398, Oct. 2009.
- [44] O. Postolache, M. D. Pereira, H. G. Ramos and A. L. Ribeiro, "NDT on aluminum aircrafts plates based on eddy current sensing and image processing," in *2008 IEEE International Instrumentation and Measurement Technology Conference*, May 2008, pp.1803-1808.
- [45] M. Li, S. D. Holland and W. Q. Meeker, "Statistical methods for automatic crack detection based on vibrothermography sequence-of-images data," *Appl. Stochastic Models Bus. Ind.*, vol. 26, pp. 481-495, 2010.
- [46] V. Kaftandjian, O. Dupuis, D. Babot and Y. M. Zhu, "Uncertainty modelling using

- Dempster–Shafer theory for improving detection of weld defects,” *Pattern Recognition Letters*, vol. 24, no. 1–3, pp. 547-564, Jan. 2003.
- [47] S. K. Ho, R. M. White and J. Lucas, “A vision system for automated crack detection in welds,” *Meas. Sci. Technol.*, vol. 1, no. 3, pp. 287, 1990.
- [48] F. C. Sham, N. Chen and L. Long, “Surface crack detection by flash thermography on concrete surface,” *NDT and Condition Monitoring, Journal of the British Institute of NDT*, vol. 50, no. 5, pp. 240-243, 2008.
- [49] A Gayer, A Saya and A Shiloh, “Automatic recognition of welding defects in real-time radiography,” *NDT International*, vol. 23, no. 3, pp. 131-136, Jun. 1990.
- [50] T. W. Liao, Y. Li, “An automated radiographic NDT system for weld inspection: Part II--Flaw detection,” *NDT&E International*, vol. 31, no. 3, pp. 183-192, 1998.
- [51] G. Wang and T.W. Liao, “Automatic identification of different types of welding defects in radiographic images,” *NDT&E International*, vol. 35, no. 8, pp. 519-528, 2002.
- [52] A. Ayenu-Prah and N. Atttoh-Okine, “Evaluating pavement cracks with bidimensional empirical mode decomposition,” *EURASIP Journal on Advances in Signal Processing 2008*, vol. 2008, pp. 1-7, 2008.
- [53] U. Park, L. Udpa and G. C. Stockman, “Motion-based filtering of magneto-optic imagers,” *Image and Vision Computing*, vol. 22, no. 3, pp. 243–249, 2004.
- [54] M.S. Mansoory, N, H. Tajik and M. Pashna, “Surface defect isolation in ceramic tile based on texture feature analysis using radon transform and FCM,” in *2009*

- International Conference on Signal Processing Systems*, May 2009, pp.85-90.
- [55] X. Zhang, Y. Li, X. Lin, M. Liu and J. Xu, “The research of defects detection and segmentation for weld radiographic inspection,” *Visual Communications and Image Processing 2005*, vol. 5960, Jul. 2005.
- [56] T. Saar and O. Talvik, “Automatic asphalt pavement crack detection and classification using neural networks,” in *12th Biennial Baltic Electronics Conference*, Oct. 2010, pp. 345-348.
- [57] “Standard Reference Photographs for Liquid Penetrant Inspection”, ASTM E433-71, 2003.
- [58] “Methods for Liquid Penetrant Examination”, ASTM SE-165.
- [59] “Colony Collapse Disorder Progress Report”, Agricultural Research Service, United States Department of Agriculture, 2010.
- [60] “CAPA Statement on Honey Bees Losses in Canada”, Canadian Association of Professional Apiculturists, 2009.
- [61] T. Stankus, “A review and bibliography of the literature of honey bee colony collapse disorder: a poorly understood epidemic that clearly threatens the successful pollination of billions of dollars of crops in America,” *Journal of Agricultural & Food Information*, vol. 9, no. 2, pp. 115-143, 2008.
- [62] D. L. Cox-Foster, S. Conlan and E. C. Holmes, “A metagenomic survey of microbes in honey bee colony collapse disorder,” *Science*, vol. 318, no. 5848, pp. 283-287, Oct. 2007.

- [63] “Foul Brood Disease of Honey Bees,” The Food and Environment Research Agency, UK., <https://secure.fera.defra.gov.uk>.
- [64] D.C. de Graaf, A.M. Alippi, M. Brown, etc., “Diagnosis of American foulbrood in honey bees: a synthesis and proposed analytical protocols,” *2006 The Society for Applied Microbiology, Letters in Applied Microbiology*, vol. 43, no. 6, pp. 583–590, 2006.
- [65] E. Guzmán-Novoa, L. Eccles, Y. Calvete, J. McGowan, P. G. Kelly, A. Correa-Benitez, “*Varroa destructor* is the main culprit for the death and reduced populations of overwintered honey bee (*Apis mellifera*) colonies in Ontario, Canada,” *Apidologie*, vol. 41, num. 4, pp. 443-450, 2010.
- [66] T.R. Copley, H.Chen, P. Giovenazzo, E. Houle, S.H. Jabaji, “Prevalence and seasonality of *Nosema* species in Québec honey bees,” *The Canadian Entomologist*, vol. 144, no. 4, pp. 1-12, 2012.
- [67] C. Chen, E. Yang, J. Jiang and T. Lin, “An imaging system for monitoring the in-and-out activity of honey bees,” *Computers and Electronics in Agriculture*, vol. 89, pp. 100-109, 2012.
- [68] M. Ramírez, J. P. Prendas, C. M. Travieso, R. Calderón and O. Salas, “Detection of the mite *Varroa destructor* in honey bee cells by video sequence processing,” in *IEEE 16th International Conference on Intelligent Engineering Systems*, Jun. 2012, pp. 103-108.
- [69] L. Liew, B. Y. Lee and M. Chan, “Cell detection for bee comb images using circular Hough transformation,” in *2010 International Conference on Science and Social*

Research (CSSR 2010), Dec. 2010, pp. 191-195.

- [70] A. Fitzgibbon, M. Pilu, and R. B. Fisher, "Direct least square fitting of ellipses," *Pattern Analysis and Machine Intelligence*, vol. 21, no. 5, pp. 476-480, 1999.